Title: Diverse viral *cas* genes antagonize CRISPR immunity

Authors: Mark A Katz[1], Edith M Sawyer[1], Albina Kozlova[1], Madison C Williams[1], Shally R Margolis[1], Luke Oriolt[1], Matthew Johnson[2], Joseph Bondy-Denomy[2], Alexander J Meeske[1]

Affiliations:
[1]Department of Microbiology, University of Washington, Seattle, WA 98109, USA.
[2]Department of Microbiology and Immunology, University of California, San Francisco, San Francisco, CA 94158, USA.

Correspondence: meeske@uw.edu

ABSTRACT

Prokaryotic CRISPR-Cas immunity is subverted via anti-CRISPRs (Acrs), small proteins that inhibit Cas protein activities when expressed during the phage lytic cycle or from resident prophages or plasmids. CRISPR-Cas defenses are classified into 6 types and 33 subtypes, which employ a diverse suite of Cas effectors and differ in their mechanisms of interference. As Acrs often work via binding to a cognate Cas protein, inhibition is almost always limited to a single CRISPR type. Furthermore, while *acr* genes are frequently organized together in phage-associated gene clusters, how such inhibitors initially evolve has remained unclear. Here we have investigated the Acr content and inhibition specificity of a collection of *Listeria* isolates, which naturally harbor four diverse CRISPR-Cas systems (types I-B, II-A, II-C, and VI-A). We observed widespread antagonism of CRISPR, which we traced to 12 novel and 4 known Acr gene families encoded on endogenous mobile genetic elements. Among these were two Acrs that possess sequence homology to type I-B Cas proteins and assemble into a defective interference complex. Surprisingly, an additional type I-B Cas homolog did not affect type I immunity, but instead inhibited the RNA-targeting type VI CRISPR system through sequestration of crRNA. By probing the IMGVR database of viral genomes, we detected abundant orphan *cas* genes located within putative anti-defense gene clusters. We experimentally verified the Acr activity of one viral *cas* gene, a particularly broad-spectrum *cas3* homolog that inhibits type I-B, II-A, and VI-A CRISPR immunity. Our observations provide direct evidence of Acr evolution via *cas* gene co-option, and new genes with potential for broad-spectrum control of genome editing technologies.

MAIN

Prokaryotic CRISPR-Cas systems use RNA-guided Cas nucleases to provide their hosts with sequence-specific immunity against foreign genetic elements, such as bacteriophages and plasmids[1,2]. Small fragments of foreign DNA are captured and integrated as “spacer” sequences in the CRISPR locus, which is then transcribed and processed into mature crRNAs[3,4]. These RNAs guide Cas nucleases in recognition and cleavage of matching targets in foreign nucleic acids[1,2,5]. In response to the strong selective pressure imposed by CRISPR immunity, phages and other mobile genetic elements have evolved anti-CRISPR proteins (Acrs), which antagonize the immune effector activities of Cas proteins, removing the barrier to infection[6]. Acrs work via diverse mechanisms to inhibit critical steps of CRISPR immunity, including *cas* gene expression[7,8], assembly of CRISPR ribonucleoprotein complexes[9,10], recognition of target nucleic acids[11,12], and recruitment of effector nucleases[11]. CRISPR-Cas systems are highly diverse immune modules that differ in their *cas* gene sequences, organization, and mechanism of target interference[13]. Most characterized Acrs act via a protein-protein interaction with their cognate Cas protein, and therefore inhibition specificity is almost always limited to a single CRISPR subtype.

How *acr* genes arise within phage genomes is not well understood. While some Acrs have enzymatic activity and likely evolved from enzymes sharing the same fold, a lack of detectable protein homology for most Acrs limits our ability to understand their origins[10,14-16]. One Acr (AcrIF3) has been shown to mimic the structure of the Cas protein Cas8f to block recruitment of the type I-F CRISPR nuclease Cas2-3[17,18]. AcrIF3 does not bear significant sequence homology to Cas8f, therefore it is unknown whether this is a case of convergent evolution, or if the two proteins share a common ancestor but have diverged to the point of unrecognizable similarity. Many archaeal viruses encode homologs of Cas4, which normally plays a role in processing newly acquired spacers[19-21]. Some experimental evidence suggests viral Cas4 proteins inhibit spacer acquisition, suggesting that *cas* genes might be co-opted by viruses for CRISPR antagonism[22]. While viral CRISPR-Cas systems are diverse and abundant[23], no viral *cas* gene has been shown to inhibit the interference stage of immunity, and the extent of *acr* evolution from *cas* genes has not been explored.

Listeria spp. have evolved a diverse suite of immune defenses, including four types of CRISPR-Cas systems, to defend against abundant invading phages and mobile genetic elements[24]. The foodborne pathogen *Listeria monocytogenes* is a target of phage-mediated biocontrol efforts, and understanding the anti-defense arsenal of *Listeria* phages holds the potential to enhance this approach[25]. Previous studies have uncovered Acrs encoded by *Listeria* phages, including six that inhibit type II-A and one that inhibits the type VI-A CRISPR-Cas system[9,12,26]. Genes encoding these inhibitors are often clustered together in operons, located downstream of phage lysin genes, or within plasmids. Here we investigated the frequency of endogenous Acr-mediated inhibition by screening the functionality of 4 CRISPR types across 62 strains of *Listeria seeligeri.* We bioinformatically predicted *acr* gene candidates and tested them, guided by the results of our functional screen. These efforts uncovered 12 novel *acr* gene

84 families (7 type I-B, 3 type II-C, 2 type VI-A). We found that 3 of these genes bear
85 sequence similarity to type I-B *cas* genes. Two of them (AcrIB3 and AcrIB4) inhibit type
86 I-B by assembling into a defective interference complex. The other (AcrVIA2) is a Cas3
87 homolog that inhibits the loading, processing, or stability of Cas13-associated crRNAs.
88 Finally, we performed a bioinformatic search for orphan *cas* genes in viral genomes,
89 revealing 358 putative anti-defense loci anchored by a diverse set of type I, II, III, IV,
90 and VI *cas* genes. We experimentally verified one of them in *Listeria,* a Cas3 homolog
91 exhibiting particularly broad-spectrum inhibitory activity against type I-B, VI-A, and II-A
92 CRISPR immunity. Overall, our results exemplify the complex phage-bacteria arms
93 race, and support a mechanism for frequent *acr* gene evolution from *cas* genes.
94
95
96 **Variation in *Listeria seeligeri* genomes affects CRISPR-Cas function.**

97 CRISPR-Cas loci can be readily identified by analysis of microbial genome sequences.
98 However, whether these systems provide functional immunity cannot be inferred from
99 sequence analysis alone. We previously established *Listeria seeligeri* as a tractable
100 model for studying type VI-A CRISPR-Cas immunity, and found that *L. seeligeri* strains
101 are also richly populated with type I-B, II-A, II-C CRISPR systems, along with many
102 prophages and plasmids[12,24,27,28]. We sought to determine the extent to which resident
103 mobile genetic elements and prophages affect the function of all four *Listeria* CRISPR-
104 Cas types. We cloned each type into the site-specific integrating vector pPL2e[29] under
105 the control of a constitutive promoter, and equipped each with a spacer recognizing a
106 target plasmid (Fig. 1A). We first introduced each of these constructs into *L. seeligeri*
107 strain LS1 and confirmed that all four were capable of mediating sequence-specific
108 interference against a target plasmid that was introduced by conjugation (Fig 1B). Next,
109 we integrated each plasmid-targeting CRISPR-Cas construct into 54 out of the 62 *L.*
110 *seeligeri* strains in our laboratory's collection, then challenged each of the 216 resultant
111 strains with a cognate target plasmid (Fig. 1C-D and Figs. S1-4). While each CRISPR
112 type remained functional in some of the recipient strains, we observed frequent loss of
113 CRISPR function among the different genetic backgrounds. The loss of CRISPR
114 function we observed for each type did not correlate with the natural occurrence of that
115 type in the tested strains (Fig 1E). We observed either a partial or complete loss of
116 CRISPR-Cas system function in 29% of strains assessed for type VI-A activity, 77%
117 tested for type I-B activity, 36% tested for type II-A activity, and 39% tested for type II-C
118 activity. In some cases, we were unable to determine whether a particular CRISPR type
119 was inhibited, due to low conjugation efficiency of both the target plasmid and a non-
120 targeted control (Fig. 1B, gray bars). The strains tested were least likely to support the
121 function of type I-B, the most common *L. seeligeri* CRISPR type, while most supported
122 the function of type VI-A, which is less abundant. In contrast, type II-C is the rarest type
123 among L. seeligeri strains, yet it frequently lost function when integrated into our tested
124 strains. Collectively, our findings indicate that variation in genetic background affects the
125 function of all four CRISPR types found in *Listeria spp*.

126

127 **Identification of type I-B, II-A, II-C, and VI-A anti-CRISPR proteins.**

128 While the results above could be explained by the variable presence of unknown host
129 factors required for CRISPR-Cas function, we hypothesized that the four CRISPR types
130 might also be inhibited by anti-CRISPR proteins endogenously expressed by the strains
131 in our collection. To identify such inhibitors, we took an iterative guilt-by-association
132 bioinformatic approach that was guided by the results of our functional screen. Six type
133 II-A inhibitor proteins and one type VI-A inhibitor have been previously identified in
134 *Listeria* phage genomes, and Acr genes are frequently clustered in operons associated
135 with prophages or other mobile genetic elements. Therefore, we tested genes located
136 within predicted Acr clusters for the ability to inhibit CRISPR types that could no longer
137 mediate interference when transplanted into the cluster's host genome. First, we
138 searched each of the *L. seeligeri* genomes in our collection for genes homologous to 81
139 known Acrs, which resulted in the identification of 25 predicted Acr loci. (Table S2). We
140 examined the genes predicted to be in the same operon as known Acrs in these loci,
141 generating a list of 33 putative anti-defense candidate gene families. Using these new
142 candidates as queries, we searched the genomes again to find new putative anti-
143 defense loci and anti-defense candidate genes, giving priority to genes located between
144 previously identified candidates. We also identified predicted loci and candidate genes
145 by searching *Listeria* genomes available in the NCBI nr and wgs databases. By
146 exhaustively iterating this process, we expanded our dataset to 55 predicted anti-
147 defense loci and 76 anti-defense candidate gene families residing within the 62 *L.*
148 *seeligeri* genomes in our collection (Fig. S5, Table S2).

149 Next, we investigated whether the Acr content of each host strain correlated with loss of
150 function for each transplanted CRISPR type (Figs. S5-9). No known type I-B inhibitors
151 exist in *Listeria*. However, of the 13 strains that did not support type II-A CRISPR
152 function, all encoded at least one previously identified type II-A Acr (Fig. S7).
153 Conversely, only 2 of the 32 strains supporting type II-A function contained a cognate
154 *acr* gene. Furthermore, AcrIIA1 inhibits both type II-A and type II-C immunity[8], and was
155 present in 10 of the 15 strains lacking type II-C function (Fig. S8). Finally, the only
156 known type VI-A *acr* (*acrVIA1*) in *Listeria* was present in a genome incompatible with
157 type VI-A interference, and was absent from all other genomes (Fig. S9). These data
158 suggest that the loss of CRISPR function observed in our screen can largely be
159 explained by host-encoded Acrs. We identified anti-defense candidate genes
160 specifically present in strains that inhibited types I-B, II-C, and VI-A, and expressed
161 each from a plasmid in strain LS1, which does not harbor any anti-CRISPR genes. We
162 then tested whether each candidate inhibited the matching CRISPR type in our plasmid
163 targeting assay (Fig. 2A). We prioritized testing of candidates that were present in
164 inhibitory strains for a given CRISPR type but absent from strains that tolerated function
165 of that type. We ultimately cloned 43 candidate genes, as well as 7 previously identified
166 *acr* genes, and tested each for inhibition of all four CRISPR types (Fig. 2B-C). Of the
167 tested novel candidates, 7 inhibited type I-B (hereafter *acrIB3-9*), 3 inhibited type II-C
168 (*acrIIC7-9*), and 2 inhibited type VI-A CRISPR immunity (*acrVIA2-3*) (see Table S2 for
169 protein sequences). Each of these Acrs were tested against each CRISPR type, but
170 specifically inhibited only one of the 4 types. We also noted that a *L. seeligeri* homolog
171 of the AcrIIA3 protein tested in our assay was a potent inhibitor of type II-C CRISPR,
172 and did not inhibit type II-A, despite being 94.3% identical to *L. monocytogenes* AcrIIA3.
173 While more than one Acr might be active in a given genome, the previously identified

174 and newly discovered Acrs could collectively account for 68% of the inhibition observed
175 in our functional screen.

176 In total, we discovered 12 new Acr families, 11 of which each had several homologs
177 present in a variety of *Listeria* species and phages (Fig. 2D, Fig. S10). The occurrence
178 of these *acr* genes was limited to *Listeria*, except for AcrIIC9, which was also found in
179 other *Firmicutes,* notably *Enterococcus.* Genes encoding homologs of AcrIB3, AcrIB4,
180 AcrIB7, AcrIB8, AcrIIC7, AcrIIC8, and AcrVIA2 were found in mobile genetic elements
181 within *Listeria* genomes, while AcrIB5, AcrIB6, AcrIB7, AcrIB9, AcrIIC9, and AcrVIA3
182 were found in *Listeria* phage genomes. Few of these Acr proteins contained domains of
183 known function, however, we noted that four of them contained HTH domains predicted
184 to mediate DNA binding. Indeed, in addition to its CRISPR inhibition discovered here,
185 we previously demonstrated that the gene encoding AcrIIC9 functions as a negative
186 autoregulator of its own *acr* gene locus[12]. Finally, three of the Acrs shared sequence
187 homology with type I-B Cas proteins, which we discuss in detail below.

188

189 **Cascade component homologs inhibit type I-B CRISPR-Cas immunity.**

190 Two of the newly discovered type I-B Acr proteins (AcrIB3 and AcrIB4) shared
191 sequence homology with two type I-B Cas proteins (Cas5 and Cas8b, respectively) that
192 assemble into the Cascade complex (Fig. 3A). The AcrIB3 protein shares 38% amino
193 acid identity with the full-length Cas5 protein (Fig. S11A), while the AcrIB4 protein
194 shares 38% amino acid identity with the last 90 residues of the 562aa Cas8b protein
195 (Fig. S11B). We hypothesized that AcrIB3 and AcrIB4 might inhibit type I-B CRISPR
196 immunity by acting as faulty subunits integrated within the Cascade complex. An
197 alternative possibility is that expression of any individual natural Cas protein from a
198 multi-copy plasmid would interfere with Cascade complex assembly via disruption of
199 subunit stoichiometry. To test whether this was the case, we separately expressed
200 AcrIB3, AcrIB4, and their cognate Cas protein homologs Cas5 and Cas8b, and tested
201 their effect on plasmid targeting by the type I-B CRISPR system (Fig. 3B). While the two
202 Acrs potently inhibited interference against the target plasmid, neither *bona fide* Cas
203 protein impacted immunity. We performed BLAST searches of AcrIB3 and AcrIB4
204 against the NCBI nr database. In addition to numerous true Cas5 and Cas8b protein
205 homologs, we uncovered 45 and 49 unique homologs (respectively) which were not
206 located within CRISPR-Cas loci, and all limited to *Listeria spp*. (Fig. 3C). Our
207 phylogenetic analysis of the proteins uncovered by this search indicated that both Acrs
208 form their own high-confidence clades, suggesting an ancient divergence from their
209 cognate Cas proteins. We therefore conclude that AcrIB3 and AcrIB4 are Cas protein
210 homologs that function as inhibitors of the type I-B CRISPR-Cas system.

211 To investigate the mechanism by which AcrIB3 and AcrIB4 inhibit type I-B CRISPR
212 immunity, we first tested whether they affected target DNA engagement by the Cascade
213 complex (Fig. 3D). We designed a CRISPRi-like assay in which we deleted the
214 nuclease *cas3* from the CRISPR locus, then targeted Cascade to a plasmid-borne *lacZ*
215 reporter gene in *L. seeligeri* LS1. Inactivation of *cas3* ensures that target DNA bound by

216 Cascade will not be cleaved. When we probed for *lacZ* activity by growth on plates
217 containing X-gal, we observed CRISPR-dependent transcriptional silencing of the
218 targeted *lacZ* gene. When we co-expressed either AcrIB3 or AcrIB4 along with
219 Cascade, *lacZ* transcription was restored, suggesting that both anti-CRISPRs act
220 upstream of target DNA binding by the Cascade complex, and that neither function at
221 the level of Cas3 recruitment. Consistent with our previous observations, neither Cas5
222 nor Cas8b influenced target DNA recognition.

223 Next, we investigated whether AcrIB3 and/or AcrIB4 affect assembly of the Cascade
224 complex. We began by constructing a type I-B CRISPR locus containing a *cas6* allele
225 fused to a 3xFlag tag on the C-terminus. We confirmed that this fusion remained
226 functional in interference against a plasmid with a type I-B protospacer (Fig. S13A). We
227 then used this construct to perform anti-Flag immunoprecipitations of the Cascade
228 complex, in the presence and absence of AcrIB3 and AcrIB4. In the absence of Acrs,
229 the silver-stained Cas6-3xFlag immunoprecipitate fraction contained bands consistent
230 with the molecular weights of Cas8b, Cas7, Cas6, and Cas5, none of which were
231 present in a untagged control sample (Fig. 3E). When we co-expressed AcrIB3 or
232 AcrIB4, each Cascade subunit remained present in the immunoprecipitate, suggesting
233 that neither Acr impedes assembly of the type I-B Cascade complex. To test whether
234 AcrIB3 was integrated into the complex, we fused an N-terminal his6 tag onto AcrIB3,
235 confirmed that it was functional in inhibition of plasmid targeting by type I-B CRISPR,
236 and performed immunoprecipitation of the Cascade complex in the presence of his6-
237 AcrIB3 (Fig. 3F, Fig. S13b). We then analyzed the contents of the load, unbound, and
238 immunoprecipitated fractions by immunoblotting for Cas6-3xFlag, His6-AcrIB3, and the
239 housekeeping sigma factor σ^A. We found that His6-AcrIB3 (but not σ^A) strongly co-
240 immunoprecipitated with Cas6-3xFlag, suggesting that AcrIB3 assembles into the
241 Cascade complex. While we attempted to perform the same experiment with AcrIB4, we
242 could not obtain a functional tagged allele.

243

244 **A Cas3 homolog inhibits type VI-A CRISPR immunity at the crRNA biogenesis**
245 **stage.**

246 In addition to AcrIB3 and AcrIB4, we discovered a third Acr protein (AcrVIA2) with
247 homology to type I-B Cas proteins (Fig. 4A). AcrVIA2 shares 24% sequence identity
248 with the helicase-nuclease Cas3 (Fig. S12). The homology between the two proteins is
249 centered on a shared DEAD-box helicase domain, and AcrVIA2 lacks the HD nuclease
250 domain of Cas3. Our homology searches uncovered several true Cas3 proteins as well
251 as 8 predicted AcrVIA2 homologs not located near a CRISPR array or *cas* gene operon,
252 2 of which were present on *Listeria* mobile genetic elements, while the rest were
253 encoded in *Myoviridae* phage genomes (Fig. 4B). Again, the Acrs formed a high-
254 confidence phylogenetic group separate from true Cas3 proteins. Surprisingly, we found
255 that this Acr did not inhibit type I-B immunity, but instead strongly inhibited the RNA-
256 targeting type VI-A CRISPR system (Fig. 2C). As with the two previously mentioned
257 Cas-homolog Acrs, we confirmed that *bona fide* Cas3 possessed no inhibitory activity
258 against Cas13 in a plasmid-targeting assay (Fig. 4C). When we mutated the AcrVIA2

259 DEAD box (DEFD>AAFD), we found that it lost inhibitory activity, suggesting that this
260 domain is required for the function of AcrVIA2 (Fig. 4C). Next, we tested whether
261 AcrVIA2 could prevent Cas13 immunity against a phage target (Fig. 4D). We infected
262 lawns of *L. seeligeri* harboring a spacer (*spc59*) targeting the Cas13-sensitive phage
263 ϕLS59, while co-expressing AcrVIA2 from a plasmid. While we observed a CRISPR-
264 dependent reduction in ϕLS59 plaque formation in this system, expression of AcrVIA2
265 restored phage infection in the presence of Cas13 immunity. Finally, recognition of
266 target RNA by Cas13 stimulates a non-specific *trans*-RNase activity that induces cell
267 dormancy in *L. seeligeri*[28]. We tested whether AcrVIA2 impacts activation of Cas13
268 *trans* activity using a strain harboring an aTc-inducible, non-essential, non-coding RNA
269 containing a protospacer recognized by *spc4* of the type VI-A CRISPR array (Fig. 4E).
270 This strain is viable in the absence of target induction, but when plated on media
271 containing aTc, exhibits a strong Cas13-dependent growth defect as a consequence of
272 nonspecific RNase activity. In contrast, co-expression of AcrVIA2 abolished Cas13-
273 induced dormancy, and therefore prevents cleavage of target and non-target RNA.

274 Next we investigated the mechanism of Cas13 inhibition by AcrVIA2. We first attempted
275 to detect a physical interaction between both proteins. However, we were unable to
276 detect co-immunoprecipitation of Cas13-his6 along with a partially functional AcrVIA2-
277 3xflag allele (Fig. S14), suggesting that, unlike AcrVIA1, AcrVIA2 does not form a stable
278 interaction with Cas13. Accordingly, we tested whether AcrVIA2 impacts the assembly
279 of the Cas13:crRNA RNP complex. We immunoprecipitated a functionally tagged
280 Cas13-3xFlag allele in the presence and absence of AcrVIA2, then purified RNA from
281 the isolated protein and analyzed it by SYBR Gold staining (Fig. 4F). We detected an
282 RNA band consistent with the mature 51 nt crRNA in the immunoprecipitated Cas13
283 fraction, but this band was absent from the protein purified from cells expressing
284 AcrVIA2. Conversely, neither the AcrVIA2 DEAD-box mutant nor the unrelated protein
285 AcrVIA3 affected Cas13-associated crRNA levels. Collectively, these results suggest
286 that AcrVIA2 influences type VI-A crRNA processing, loading, or stability, in a
287 mechanism that depends on its DEAD-box motif.

288

289 **Diverse viral *cas* genes reside in putative anti-defense loci.**

290 Our discovery of 3 unique Acrs homologous to type I-B Cas proteins prompted us to
291 perform bioinformatic searches for other viral *cas* genes that might play anti-defense
292 roles. We used 536 Cas protein query sequences to probe for *cas* genes present in the
293 IMGVR database of high-confidence viral genomes. To enrich for putative Acrs, we then
294 removed all hits containing nearby predicted CRISPR arrays or high-confidence *cas*
295 gene operons. We further eliminated all genes located within 1 kb of DNA contig ends,
296 and genes that shared greater than 90% nucleotide sequence identity with an existing
297 hit. Ultimately, our analysis yielded 358 predicted orphan viral *cas* genes, representing
298 components of types I, II, III, IV, and VI CRISPR-Cas systems (Fig. 5A, Table S3). The
299 predicted hosts infected by viruses harboring orphan *cas* genes included most bacterial
300 phyla, with *Firmicutes* and *Bacteroidota* phages being particularly abundant. We found
301 that several of the predicted viral *cas* genes were located next to known *acr* genes or

302 predicted anti-defense candidates from our analysis in *Listeria*, supporting the idea that
303 some of the *cas* homologs in our dataset play anti-CRISPR roles (Fig. 5B and Fig. S15).

304 To investigate this, we selected *acr* gene candidates with homology to *Listeria cas*
305 genes, and tested their ability to inhibit plasmid targeting by each CRISPR type (Fig.
306 5C-D). Among the tested candidates was a *cas3* homolog encoded on a *Myoviridae*
307 genome. Like AcrVIA2, this protein shared limited identity (~24%) with the DEAD-box
308 helicase domain of *L. seeligeri* Cas3, shared less than 40% sequence identity with
309 AcrVIA2 (Fig. 5C), and contained no additional domains of known function. Finally,
310 while AcrVIA2 is similar in length to Cas3, the viral Cas3 homolog identified in our
311 bioinformatic search was over twice the size, at 1,128 amino acids. We first the viral
312 Cas3 homolog's ability to inhibit type VI-A CRISPR immunity against a targeted
313 plasmid, and found that it abolished Cas13-dependent interference. Due to its homology
314 to AcrVIA2, we refer to it as AcrVIA2.1. Next, we tested the inhibition spectrum of
315 AcrVIA2.1 against the four *Listeria* CRISPR-Cas types (Fig. 5D). Unlike AcrVIA2,
316 AcrVIA2.1 mediated strong inhibition of types VI-A, I-B, and II-A CRISPR interference.
317 Thus, of all anti-CRISPRs characterized to date, AcrVIA2.1 has both the largest size
318 and Cas protein inhibition spectrum. Collectively, our results suggest that there has
319 been extensive *acr* evolution from *cas* genes, and that searching for orphan *cas* genes
320 homologs in viral genomes is a useful approach to bioinformatically identify new anti-
321 defense gene loci.

322

323 **DISCUSSION**

324 Here we have investigated the occurrence of anti-CRISPR-mediated inhibition across a
325 large collection of bacterial isolates, and four CRISPR-Cas types. Our results suggest
326 the existence of widespread CRISPR antagonism present among *Listeria seeligeri*
327 strains, which can be accounted for by 4 known and 12 previously unidentified Acr
328 families. Three of these Acrs bear sequence identity to type I-B Cas subunits,
329 suggesting that each Acr shares a common ancestor with its cognate Cas component.
330 Our investigation of the mechanisms of these Acrs indicate that (i) AcrIB3 and AcrIB4
331 inhibit type I-B CRISPR immunity via assembly into a defective Cascade interference
332 complex that fails to engage target DNA, and (ii) AcrVIA2 inhibits type VI-A CRISPR
333 immunity by blocking the processing, loading, or stability of Cas13-associated crRNA.
334 To investigate the generality of Acr evolution from Cas proteins, we probed the IMGVR
335 database for the existence of orphan viral *cas* genes. We uncovered hundreds of
336 examples of viral *cas* genes that were not associated with a CRISPR array or complete
337 *cas* gene operon, instead residing near putative anti-defense genes. We experimentally
338 confirmed that at least one of these genes (AcrVIA2.1) exhibits exceptionally broad-
339 spectrum inhibition of CRISPR-Cas immunity in *L. seeligeri*. In addition to uncovering
340 numerous anti-CRISPR proteins that could potentiate phage therapy or gene editing
341 safety, our findings demonstrate that diverse viruses have co-opted *cas* genes for
342 CRISPR antagonism, and provide a new strategy for the unbiased identification of
343 counter-defense genes in prokaryotes.

344 Our results raise several questions regarding the evolutionary trajectories that could
345 convert a host-encoded *cas* gene to a phage-encoded *acr.* First, how do phages
346 capture *cas* genes? One possibility is via imprecise excision of temperate phages
347 integrated near CRISPR-Cas loci. During induction of such prophages, *cas* genes could
348 occasionally be packaged into viral capsids along with the phage genome. Varble and
349 colleagues[30] recently demonstrated that some *Streptococcus* phages integrate directly
350 into the degenerate repeats of type II-A CRISPR arrays, and can sometimes capture
351 and mobilize spacer sequences. It remains to be seen whether such a mechanism
352 could also promote viral capture of whole *cas* genes or fragments thereof. Once a *cas*
353 gene is integrated into a phage genome, it may not immediately play a role in CRISPR
354 antagonism. Instead, viral *cas* genes might stimulate CRISPR immunity to play a
355 protective role for lysogenized hosts that could otherwise be infected by a second
356 phage. Next, how is a viral *cas* gene exapted into an anti-CRISPR? Because Cas
357 proteins naturally make interactions with other Cas proteins, crRNA, and target nucleic
358 acids, they are well-poised to evolve into inhibitors that block CRISPR immunity. Any
359 phage-encoded Cas protein that interacts with two or more components of the CRISPR
360 RNP might develop inhibitory activity by simply losing one of these interactions while
361 maintaining another, resulting in a faulty Cas subunit that inactivates immunity. One
362 benefit of this strategy (as compared to non-Cas anti-CRISPRs) is that it may be difficult
363 for CRISPR systems to evolve resistance against such inhibitors, since they resemble
364 the very Cas components used for immunity. Finally, our results raise the possibility that
365 subunits of anti-phage immune systems beyond CRISPR may also serve as raw
366 material for counter-defense evolution.

367 In this study, we uncovered a total of 12 anti-CRISPR families present in *Listeria*
368 prophages and mobile genetic elements. Residing beside these *acr* genes were 64
369 additional anti-defense candidate genes, 26 of which exhibited no detectable CRISPR
370 inhibition in our assay (Table S2). While some of these genes may serve other
371 functions, their frequent co-occurrence with and proximity to *acr* genes suggests that
372 many could play an anti-defense role, possibly against one or more of the other anti-
373 viral defense systems found in *Listeria spp.* Indeed, recent studies have uncovered
374 examples of viral inhibitors of CBASS, Pycsar, Thoeris, Gabija, and Hachiman
375 defenses[31-34].

376 Though CRISPR-Cas systems are abundant in *Listeria spp.*, our functional screen
377 revealed that most are inhibited by endogenous Acrs. Such frequent inhibition likely
378 provides a selective pressure to acquire new diverse immune systems not susceptible
379 to existing Acrs. For example, while we observed inhibition of the highly abundant type
380 I-B CRISPR in 77% of the tested *L. seeligeri* strains, the less common type VI-A system
381 was only inhibited in 29% of strains. If inhibition is widespread, why are CRISPR
382 systems retained by the host? On the contrary, recent evidence suggests that
383 prophage-encoded Acrs promote retention of host CRISPR-Cas systems, by preventing
384 autoimmune cleavage of targets within the integrated prophage[35]. Maintenance of
385 functional CRISPR immunity despite the presence of Acrs could provide a fitness
386 benefit in the event that the host becomes cured of the prophage or MGE harboring *acr*
387 genes. In total, our findings represent an example of the diversity of evolved interactions
388 in the ongoing phage-host arms race.

ACKNOWLEDGEMENTS

We are grateful to all members of the Meeske lab for advice and encouragement, members of the Guo and Mitchell labs for helpful discussions. This work in the AJM lab was supported by the NIH [R35GM142460, S10OD026741], NSF [FAIN2235762] and the University of Washington Royalty Research Foundation. SRM is supported by the Jane Coffin Childs Memorial Fund for Medical Research. The work in the JBD lab was supported by the National Institutes of Health (R01GM127489) and funding from the Defense Advanced Research Projects Agency (DARPA) award HR0011-17-2-0043. The views, opinions and/or findings expressed are those of the authors and should not be interpreted as representing the official views or policies of the Department of Defense or the US Government, and the DARPA Safe Genes program (HR0011-17-2-0043).

AUTHOR CONTRIBUTIONS

The project was conceived by AJM. Experiments were performed by MAK, EMS, AK, MCW, SRM, and AJM. Bioinformatic analysis was conducted by MAK, MJ, JB-D, and AJM. MJ was supervised by JB-D. The manuscript was written by MAK and AJM, all authors contributed to manuscript editing.

DECLARATION OF INTERESTS

AJM is a co-founder of Profluent Bio. J.B.-D. is a scientific advisory board member of SNIPR Biome and Excision Biotherapeutics, a consultant to LeapFrog Bio, and a scientific advisory board member and co-founder of Acrigen Biosciences. The Bondy-Denomy lab received research support from Felix Biotechnology. The other authors declare no competing interests.

REFERENCES

1. Barrangou, R., Fremaux, C., Deveau, H., Richards, M., Boyaval, P., Moineau, S., Romero, D.A., and Horvath, P. (2007). CRISPR provides acquired resistance against viruses in prokaryotes. Science *315*, 1709-1712. 10.1126/science.1138140.

2. Marraffini, L.A., and Sontheimer, E.J. (2008). CRISPR interference limits horizontal gene transfer in staphylococci by targeting DNA. Science *322*, 1843-1845. 10.1126/science.1165771.

3. Hale, C., Kleppe, K., Terns, R.M., and Terns, M.P. (2008). Prokaryotic silencing (psi)RNAs in Pyrococcus furiosus. RNA *14*, 2572-2579. 10.1261/rna.1246808.

4. Brouns, S.J., Jore, M.M., Lundgren, M., Westra, E.R., Slijkhuis, R.J., Snijders, A.P., Dickman, M.J., Makarova, K.S., Koonin, E.V., and van der Oost, J. (2008). Small CRISPR RNAs guide antiviral defense in prokaryotes. Science *321*, 960-964. 10.1126/science.1159689.

5. Garneau, J.E., Dupuis, M.E., Villion, M., Romero, D.A., Barrangou, R., Boyaval, P., Fremaux, C., Horvath, P., Magadan, A.H., and Moineau, S. (2010). The

428 CRISPR/Cas bacterial immune system cleaves bacteriophage and plasmid DNA.
429 Nature *468*, 67-71. 10.1038/nature09523.

430 6. Bondy-Denomy, J., Pawluk, A., Maxwell, K.L., and Davidson, A.R. (2013).
431 Bacteriophage genes that inactivate the CRISPR/Cas bacterial immune system.
432 Nature *493*, 429-432. 10.1038/nature11723.

433 7. Marino, N.D., Talaie, A., Carion, H., Zhang, Y., Silas, S., Li, Y., and Bondy-
434 Denomy, J. (2022). Translation-dependent downregulation of Cas12a mRNA by
435 an anti-CRISPR protein. bioRxiv, 2022.2011.2029.518452.
436 10.1101/2022.11.29.518452.

437 8. Osuna, B.A., Karambelkar, S., Mahendra, C., Christie, K.A., Garcia, B.,
438 Davidson, A.R., Kleinstiver, B.P., Kilcher, S., and Bondy-Denomy, J. (2020).
439 Listeria Phages Induce Cas9 Degradation to Protect Lysogenic Genomes. Cell
440 Host Microbe *28*, 31-40 e39. 10.1016/j.chom.2020.04.001.

441 9. Mahendra, C., Christie, K.A., Osuna, B.A., Pinilla-Redondo, R., Kleinstiver, B.P.,
442 and Bondy-Denomy, J. (2020). Broad-spectrum anti-CRISPR proteins facilitate
443 horizontal gene transfer. Nat Microbiol *5*, 620-629. 10.1038/s41564-020-0692-2.

444 10. Knott, G.J., Thornton, B.W., Lobba, M.J., Liu, J.J., Al-Shayeb, B., Watters, K.E.,
445 and Doudna, J.A. (2019). Broad-spectrum enzymatic inhibition of CRISPR-
446 Cas12a. Nat Struct Mol Biol *26*, 315-321. 10.1038/s41594-019-0208-z.

447 11. Bondy-Denomy, J., Garcia, B., Strum, S., Du, M., Rollins, M.F., Hidalgo-Reyes,
448 Y., Wiedenheft, B., Maxwell, K.L., and Davidson, A.R. (2015). Multiple
449 mechanisms for CRISPR-Cas inhibition by anti-CRISPR proteins. Nature *526*,
450 136-139. 10.1038/nature15254.

451 12. Meeske, A.J., Jia, N., Cassel, A.K., Kozlova, A., Liao, J., Wiedmann, M., Patel,
452 D.J., and Marraffini, L.A. (2020). A phage-encoded anti-CRISPR enables
453 complete evasion of type VI-A CRISPR-Cas immunity. Science *369*, 54-59.
454 10.1126/science.abb6151.

455 13. Makarova, K.S., Wolf, Y.I., Iranzo, J., Shmakov, S.A., Alkhnbashi, O.S., Brouns,
456 S.J.J., Charpentier, E., Cheng, D., Haft, D.H., Horvath, P., et al. (2020).
457 Evolutionary classification of CRISPR-Cas systems: a burst of class 2 and
458 derived variants. Nat Rev Microbiol *18*, 67-83. 10.1038/s41579-019-0299-x.

459 14. Dong, L., Guan, X., Li, N., Zhang, F., Zhu, Y., Ren, K., Yu, L., Zhou, F., Han, Z.,
460 Gao, N., and Huang, Z. (2019). An anti-CRISPR protein disables type V Cas12a
461 by acetylation. Nat Struct Mol Biol *26*, 308-314. 10.1038/s41594-019-0206-1.

462 15. Niu, Y., Yang, L., Gao, T., Dong, C., Zhang, B., Yin, P., Hopp, A.K., Li, D., Gan,
463 R., Wang, H., et al. (2020). A Type I-F Anti-CRISPR Protein Inhibits the CRISPR-
464 Cas Surveillance Complex by ADP-Ribosylation. Mol Cell *80*, 512-524 e515.
465 10.1016/j.molcel.2020.09.015.

466 16. Sahakyan, H., Makarova, K.S., and Koonin, E.V. (2023). Search for Origins of
467 Anti-CRISPR Proteins by Structure Comparison. CRISPR J *6*, 222-231.
468 10.1089/crispr.2023.0011.

469 17. Chowdhury, S., Carter, J., Rollins, M.F., Golden, S.M., Jackson, R.N., Hoffmann,
470 C., Nosaka, L., Bondy-Denomy, J., Maxwell, K.L., Davidson, A.R., et al. (2017).
471 Structure Reveals Mechanisms of Viral Suppressors that Intercept a CRISPR
472 RNA-Guided Surveillance Complex. Cell *169*, 47-57 e11.
473 10.1016/j.cell.2017.03.012.

474 18. Rollins, M.F., Chowdhury, S., Carter, J., Golden, S.M., Miettinen, H.M., Santiago-
475 Frangos, A., Faith, D., Lawrence, C.M., Lander, G.C., and Wiedenheft, B. (2019).
476 Structure Reveals a Mechanism of CRISPR-RNA-Guided Nuclease Recruitment
477 and Anti-CRISPR Viral Mimicry. Mol Cell *74*, 132-142 e135.
478 10.1016/j.molcel.2019.02.001.

479 19. Krupovic, M., Cvirkaite-Krupovic, V., Prangishvili, D., and Koonin, E.V. (2015).
480 Evolution of an archaeal virus nucleocapsid protein from the CRISPR-associated
481 Cas4 nuclease. Biol Direct *10*, 65. 10.1186/s13062-015-0093-2.

482 20. Hudaiberdiev, S., Shmakov, S., Wolf, Y.I., Terns, M.P., Makarova, K.S., and
483 Koonin, E.V. (2017). Phylogenomics of Cas4 family nucleases. BMC Evol Biol
484 *17*, 232. 10.1186/s12862-017-1081-1.

485 21. Goodman, D.A., and Stedman, K.M. (2018). Comparative genetic and genomic
486 analysis of the novel fusellovirus Sulfolobus spindle-shaped virus 10. Virus Evol
487 *4*, vey022. 10.1093/ve/vey022.

488 22. Zhang, Z., Pan, S., Liu, T., Li, Y., and Peng, N. (2019). Cas4 Nucleases Can
489 Effect Specific Integration of CRISPR Spacers. J Bacteriol *201*.
490 10.1128/JB.00747-18.

491 23. Al-Shayeb, B., Skopintsev, P., Soczek, K.M., Stahl, E.C., Li, Z., Groover, E.,
492 Smock, D., Eggers, A.R., Pausch, P., Cress, B.F., et al. (2022). Diverse virus-
493 encoded CRISPR-Cas systems include streamlined genome editors. Cell *185*,
494 4574-4586 e4516. 10.1016/j.cell.2022.10.020.

495 24. Williams, M.C., Reker, A.E., Margolis, S.R., Liao, J., Wiedmann, M., Rojas, E.R.,
496 and Meeske, A.J. (2023). Restriction endonuclease cleavage of phage DNA
497 enables resuscitation from Cas13-induced bacterial dormancy. Nat Microbiol *8*,
498 400-409. 10.1038/s41564-022-01318-2.

499 25. Soni, K.A., Nannapaneni, R., and Hagens, S. (2010). Reduction of Listeria
500 monocytogenes on the surface of fresh channel catfish fillets by bacteriophage
501 Listex P100. Foodborne Pathog Dis *7*, 427-434. 10.1089/fpd.2009.0432.

502 26. Rauch, B.J., Silvis, M.R., Hultquist, J.F., Waters, C.S., McGregor, M.J., Krogan,
503 N.J., and Bondy-Denomy, J. (2017). Inhibition of CRISPR-Cas9 with
504 Bacteriophage Proteins. Cell *168*, 150-158 e110. 10.1016/j.cell.2016.12.009.

505 27. Meeske, A.J., and Marraffini, L.A. (2018). RNA Guide Complementarity Prevents
506 Self-Targeting in Type VI CRISPR Systems. Mol Cell *71*, 791-801 e793.
507 10.1016/j.molcel.2018.07.013.

508 28. Meeske, A.J., Nakandakari-Higa, S., and Marraffini, L.A. (2019). Cas13-induced
509 cellular dormancy prevents the rise of CRISPR-resistant bacteriophage. Nature
510 *570*, 241-245. 10.1038/s41586-019-1257-5.

511 29. Lauer, P., Chow, M.Y., Loessner, M.J., Portnoy, D.A., and Calendar, R. (2002).
512 Construction, characterization, and use of two Listeria monocytogenes site-
513 specific phage integration vectors. J Bacteriol *184*, 4177-4186.
514 10.1128/JB.184.15.4177-4186.2002.

515 30. Varble, A., Campisi, E., Euler, C.W., Maguin, P., Kozlova, A., Fyodorova, J.,
516 Rostol, J.T., Fischetti, V.A., and Marraffini, L.A. (2021). Prophage integration into
517 CRISPR loci enables evasion of antiviral immunity in Streptococcus pyogenes.
518 Nat Microbiol *6*, 1516-1525. 10.1038/s41564-021-00996-8.

519 31. Hobbs, S.J., Wein, T., Lu, A., Morehouse, B.R., Schnabel, J., Leavitt, A., Yirmiya,
520 E., Sorek, R., and Kranzusch, P.J. (2022). Phage anti-CBASS and anti-Pycsar
521 nucleases subvert bacterial immunity. Nature *605*, 522-526. 10.1038/s41586-
522 022-04716-y.

523 32. Leavitt, A., Yirmiya, E., Amitai, G., Lu, A., Garb, J., Herbst, E., Morehouse, B.R.,
524 Hobbs, S.J., Antine, S.P., Sun, Z.J., et al. (2022). Viruses inhibit TIR gcADPR
525 signalling to overcome bacterial defence. Nature *611*, 326-331. 10.1038/s41586-
526 022-05375-9.

527 33. Yirmiya, E., Leavitt, A., Lu, A., Avraham, C., Osterman, I., Garb, J., Antine, S.P.,
528 Mooney, S.E., Hobbs, S.J., Kranzusch, P.J., et al. (2023). Phages overcome
529 bacterial immunity via diverse anti-defense proteins. bioRxiv,
530 2023.2005.2001.538930. 10.1101/2023.05.01.538930.

531 34. Huiting, E., Cao, X., Ren, J., Athukoralage, J.S., Luo, Z., Silas, S., An, N., Carion,
532 H., Zhou, Y., Fraser, J.S., et al. (2023). Bacteriophages inhibit and evade cGAS-
533 like immune function in bacteria. Cell *186*, 864-876 e821.
534 10.1016/j.cell.2022.12.041.

535 35. Rollie, C., Chevallereau, A., Watson, B.N.J., Chyou, T.Y., Fradet, O., McLeod, I.,
536 Fineran, P.C., Brown, C.M., Gandon, S., and Westra, E.R. (2020). Targeting of
537 temperate phages drives loss of type I CRISPR-Cas systems. Nature *578*, 149-
538 153. 10.1038/s41586-020-1936-2.

539 36. Altschul, S.F., Gish, W., Miller, W., Myers, E.W., and Lipman, D.J. (1990). Basic
540 local alignment search tool. J Mol Biol *215*, 403-410. 10.1016/S0022-
541 2836(05)80360-2.

542 37. Notredame, C., Higgins, D.G., and Heringa, J. (2000). T-Coffee: A novel method
543 for fast and accurate multiple sequence alignment. J Mol Biol *302*, 205-217.
544 10.1006/jmbi.2000.4042.

545 38. Tamura, K., Stecher, G., and Kumar, S. (2021). MEGA11: Molecular Evolutionary
546 Genetics Analysis Version 11. Mol Biol Evol *38*, 3022-3027.
547 10.1093/molbev/msab120.

548 39. Camargo, A.P., Nayfach, S., Chen, I.A., Palaniappan, K., Ratner, A., Chu, K.,
549 Ritter, S.J., Reddy, T.B.K., Mukherjee, S., Schulz, F., et al. (2023). IMG/VR v4:
550 an expanded database of uncultivated virus genomes within a framework of
551 extensive functional, taxonomic, and ecological metadata. Nucleic Acids Res *51*,
552 D733-D743. 10.1093/nar/gkac1037.

553 40. Quinlan, A.R., and Hall, I.M. (2010). BEDTools: a flexible suite of utilities for
554 comparing genomic features. Bioinformatics *26*, 841-842.
555 10.1093/bioinformatics/btq033.

556 41. Lee, W., and Chen, S.L. (2002). Genome-tools: a flexible package for genome
557 sequence analysis. Biotechniques *33*, 1334-1341. 10.2144/02336bc04.

558 42. Russel, J., Pinilla-Redondo, R., Mayo-Munoz, D., Shah, S.A., and Sorensen, S.J.
559 (2020). CRISPRCasTyper: Automated Identification, Annotation, and
560 Classification of CRISPR-Cas Loci. CRISPR J *3*, 462-469.
561 10.1089/crispr.2020.0059.

562 43. Krüger, D.H., Schroeder, C., Hansen, S., and Rosenthal, H.A. (1977). Active
563 protection by bacteriophages T3 and T7 against E. coli B- and K-specific
564 restriction of their DNA. Mol Gen Genet *153*, 99-106. 10.1007/bf01036001.

565 44. Seemann, T. (2014). Prokka: rapid prokaryotic genome annotation.
566 Bioinformatics *30*, 2068-2069. 10.1093/bioinformatics/btu153.

567 45. Gilchrist, C.L.M., and Chooi, Y.H. (2021). clinker & clustermap.js: automatic
568 generation of gene cluster comparison figures. Bioinformatics *37*, 2473-2475.
569 10.1093/bioinformatics/btab007.

570

571 **METHODS**

572 Bacterial strains and growth conditions:

573 *L. seeligeri* strains were cultured in Brain Heart Infusion (BHI) medium at 30°C. Where
574 appropriate, BHI was supplemented with the following antibiotics for selection: nalidixic
575 acid (50 µg/mL), chloramphenicol (10 µg/mL), erythromycin (1 µg/mL), or kanamycin
576 (50 µg/mL). For cloning, plasmid preparation and conjugative plasmid transfer, *E. coli*
577 strains were cultured in Lysogeny Broth (LB) medium at 37 °C. Where appropriate, LB
578 was supplemented with the following antibiotics: ampicillin (100 µg/mL),
579 chloramphenicol (25 µg/mL), kanamycin (50 µg/mL). For conjugative transfer of *E. coli* –
580 *Listeria* shuttle vectors, plasmids were purified from Turbo Competent *E. coli* (New
581 England Biolabs) and transformed into the *E. coli* conjugative donor strains SM10 λ*pir*
582 or S17 λ*pir.* For a list of strains used in this study, see Table S1.

583 Plasmid construction and preparation:

584 All genetic constructs for expression in *L. seeligeri* were cloned into the following three
585 compatible shuttle vectors, each of which contains an origin of transfer sequence for
586 mobilization by transfer genes of the IncP-type plasmid RP4. These transfer genes are
587 integrated into the genome of the *E. coli* conjugative donor strains SM10 λ*pir* or S17
588 λ*pir.* All plasmids used in this study, along with details of their construction can be found
589 in Table S1.

590 pPL2e: ectopically integrating plasmid conferring chloramphenicol resistance in *E. coli*
591 and erythromycin resistance in *Listeria*; integrates into the $tRNA^{Arg}$ locus in the *L.*
592 *seeligeri* chromosome[29].

593 pAM8: *E. coli-Listeria* shuttle vector conferring ampicillin resistance in *E. coli* and
594 chloramphenicol resistance in *Listeria*[27].

595 pAM326: *E. coli-Listeria* shuttle vector conferring kanamycin resistance in *E. coli* and
596 *Listeria*[12].

597 Mobilizable CRISPR-Cas systems were constructed by cloning the type I-B, II-A, II-C,
598 and VI-A CRISPR-Cas loci into pPL2e, each equipped with a spacer matching a target
599 plasmid. Target plasmids were derived from pAM8. In the case of type II-A, one variant
600 of the CRISPR-Cas plasmid harbored a spacer targeting a protospacer region on pAM8
601 followed by an NGG PAM, and a separate CRISPR plasmid harbored a non-targeting
602 spacer. The same approach was taken for type II-C, except the protospacer region was
603 followed by an NNGCAA PAM. For types I-B and VI-A, naturally occurring spacers were
604 used in the CRISPR plasmid, and matching protospacers were inserted into pAM8. The
605 type I-B protospacer was preceded by a 5' CCN PAM. The type VI-A protospacer was
606 inserted into a transcribed region in the 3' UTR of the chloramphenicol resistance gene
607 of pAM8.

608 Putative anti-CRISPR constructs were assembled by cloning into NcoI/EagI digested
609 pAM551, which is derived from pAM326 and contains an aTc-inducible P_{tet} promoter.

610 <u>*E. coli – L. seeligeri* conjugation:</u>

611 All genetic constructs for expression in *L. seeligeri* were introduced by conjugation with
612 *E. coli* donor strains SM10 λ*pir* or S17 λ*pir.* 100 µL of each donor and recipient culture
613 were diluted into 10 mL of BHI medium and concentrated on a 0.45 µm porosity filter
614 disk using vacuum filtration. Filter disks were laid onto BHI agar supplemented with
615 oxacillin (8 µg/mL for pPL2e or pAM326 derived plasmids and 128 µg/mL for pAM8
616 derived plasmids) which weakens the cell wall and enhances conjugation, then
617 incubated at 37°C for 4 hours. Cells were resuspended in 2 mL BHI, serially diluted, and
618 transconjugants were selected on BHI medium containing 50 µg/mL nalidixic acid
619 (which kills donor *E. coli* but not recipient *L. seeligeri)* in addition to the appropriate
620 antibiotic for plasmid selection. Transconjugants were isolated after 2-3 days of
621 incubation at 30°C.

622 <u>Phylogenetic tree construction:</u>

623 To reconstruct Acr phylogeny, query Acr proteins were searched against the BLAST nr
624 database[36] using an E-value cutoff of $5x10^{-3}$ (for AcrIB4) or $1x10^{-4}$ (for all other Acrs).
625 The top 250 hits were aligned using T-Coffee[37]. For AcrIB4, only the C-terminal 90
626 amino acids were included for alignment, as this is the region with shared homology
627 between AcrIB4 and the much larger Cas8b. Phylogenetic trees and bootstrap values
628 were calculated using MEGA (v11)[38], using the neighbor-joining method with 1000
629 bootstrap replications.

630 <u>Co-immunoprecipitation:</u>

631 *L. seeligeri* harboring FLAG-tagged and/or His6-tagged proteins was cultured in 30 mL
632 BHI to saturation, then pelleted by centrifugation. Cells were resuspended in 1.5 mL lysis
633 buffer containing 50 mM HEPES pH 7, 150 mM NaCl, 5 mM $MgCl_2$, 5% glycerol, 1 mM

634 PMSF, and 2 mg/mL lysozyme, then incubated at 37°C for 20 min. Lysis was performed
635 by sonication, then insoluble material was pelleted by centrifugation at 15,000 rpm for 10
636 min. The clarified supernatants were sampled (load fraction), then applied to 40 µL of
637 buffer-equilibrated M2 anti-Flag antibody affinity resin (Sigma-Aldrich) and incubated at
638 4°C for 2 h. Flag resin was pelleted by centrifugation at 1,000 rpm for 1 min, and the
639 supernatant was sampled (unbound fraction). Flag resin was washed three times for 5
640 min each with 1 mL wash buffer (50 mM HEPES pH 7, 150 mM NaCl, 5 mM $MgCl_2$, 5%
641 glycerol). Finally, the immunoprecipitated fraction was eluted with 40 µL of 0.1 mg/mL
642 3xFlag peptide (Sigma-Aldrich) at room temperature. All samples were denatured by
643 dilution in 2x Laemmli sample buffer containing 4% SDS and 10% beta-mercaptoethanol.
644 Load, unbound, and IP fractions were analyzed by immunoblot using anti-Flag (Sigma-
645 Aldrich), anti-His6 (Genscript), and anti-σ^A (gift of David Rudner, Harvard Medical School)
646 antibodies. Silver staining was performed on 12 µL of each immunoprecipitate sample,
647 using the Pierce Silver Staining Kit (Thermo Fisher) according to the manufacturer's
648 instructions.

649 Analysis of Cas13-associated crRNA:

650 *L. seeligeri* cultures harboring *cas13-his6* and/or *acrVIA2* were grown to saturation. 50
651 mL culture was harvested, pelleted at 4300 rpm and frozen at -80°C. Pellets were
652 resuspended in ice-cold lysis buffer (50 mM HEPES pH7.0, 150 mM NaCl, 5mM MgCl2,
653 10 mM imidazole, 1 mg/mL lysozyme, 1 mM phenylmethylsulfonylfluoride, 5% glycerol)
654 and lysed by sonication. Lysate was centrifuged at 15,000 rpm for 15 minutes at 4°C.
655 Soluble material was batch bound for 2 hours with 50uL of Ni-NTA HisBind Resin. Resin
656 was then washed three times with 1 mL wash buffer (50 mM HEPES pH7.0, 150 mM
657 NaCl, 5mM MgCl2, 10 mM imidazole 5% glycerol) and eluted with wash buffer
658 supplemented with 250 mM imidazole. RNA was purified using the Direct-zol RNA
659 miniprep kit (Zymo Research). Samples were resolved by denaturing 15% TBE-Urea
660 PAGE, stained with SYBR Gold according to the manufacturer's instructions, and imaged
661 on an Azure Biosystems Azure 600 imager.

662 Phage propagation:

663 All phage infections were performed in BHI medium supplemented with 5 mM CaCl2. To
664 generate phage lysates, existing phage stocks were diluted to single plaques on a lawn
665 of *L. seeligeri* LS1 *ΔRM1 ΔRM2* and a single plaque was purified twice to ensure
666 homogeneity. 5 mL of cell culture was infected with phage at MOI 0.1, OD 0.1 and the
667 infection proceeded overnight. The lysate was centrifuged for 20 minutes at 4,000 rpm
668 and the supernatant was filtered using a 0.45 µm pore syringe filter.

669 Bioinformatic identification of viral *cas* genes:

670 The IMGVR7.1 database of high-confidence viral genomes[39] was probed for sequences
671 with homology to 536 Cas protein query sequences, representing all known CRISPR
672 subtypes[13]. Each query was searched against IMGVR7.1 using tblastn[36] with an E-
673 value cutoff of $1x10^{-4}$. 20 kb of genomic sequence flanking each hit gene was retrieved
674 using bedtools[40], and hits were deduplicated using genometools sequniq[41]. Hit genomic
675 regions were analyzed for *bona fide* CRISPR-Cas systems using CRISPRCasTyper[42],
676 and all hits containing either predicted CRISPR arrays or *cas* gene operons were

677 removed from analysis. Hits were further filtered to remove any *cas* genes located
678 within 1 kb of a contig end, and hits sharing greater than 90% nucleotide sequence
679 identity were collapsed using T-Coffee seq_reformat[37]. Finally, the IMGVR7.1 database
680 was probed as above for homologs of known Acrs, anti-restriction-modification[43], anti-
681 Hachiman[33], anti-Gabija, and anti-Thoeris genes, and hits within 10 kb of a predicted
682 *cas* gene were tabulated. The UViG identifier for each hit was used to retrieve predicted
683 host phylogeny from IMGVR. For gene loci diagrams, ORFs were predicted with
684 prokka[44] and diagrams were generated with Clinker[45].

685

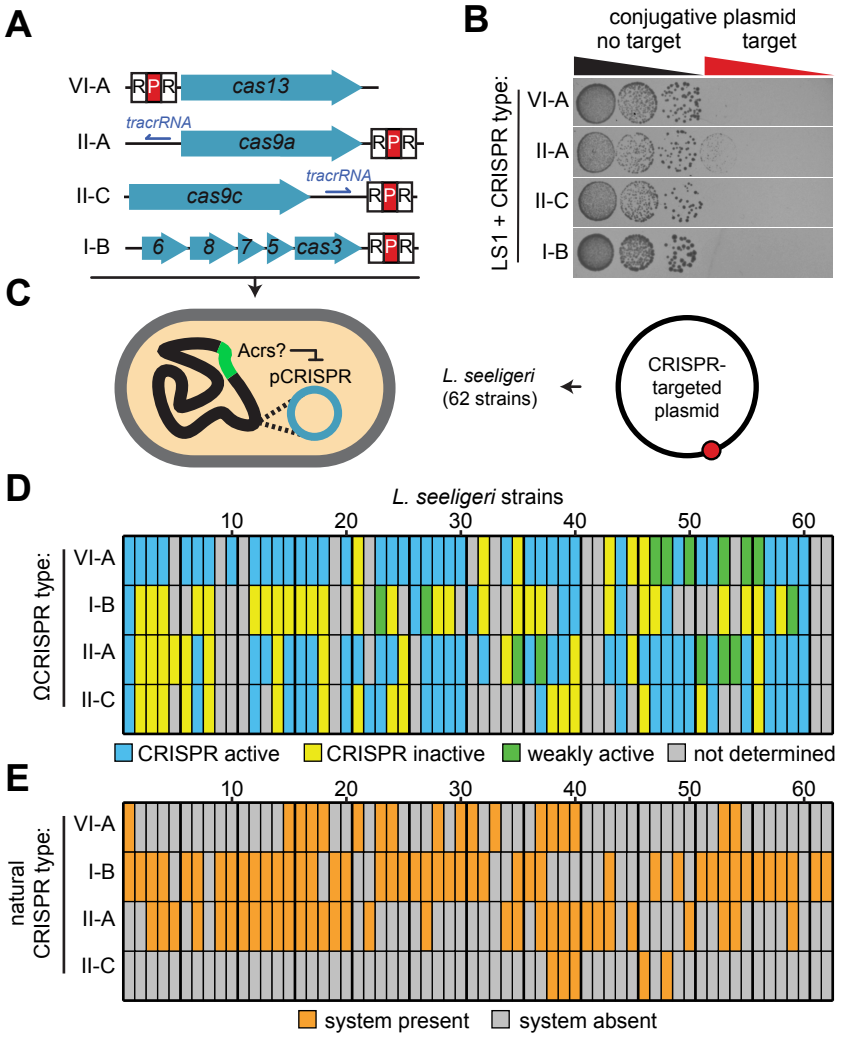

Figure 1. Variation in L. seeligeri genomes affects CRISPR-Cas function. (A) Schematic of mobilizable chromosomally-integrating CRISPR-Cas loci each equipped with a single plasmid-targeting spacer. **(B)** Plasmid targeting assay demonstrating sequence-specific interference by all four CRISPR-Cas types in strain LS1. **(C)** Schematic of strategy to detect activity of endogenous Acrs by introducing CRISPR-Cas loci into diverse strain backgrounds and challenging them with target plasmid. **(D)** Functionality of 4 CRISPR types across 62 L. seeligeri strains. **(E)** Natural occurrence of CRISPR types across the strain collection.

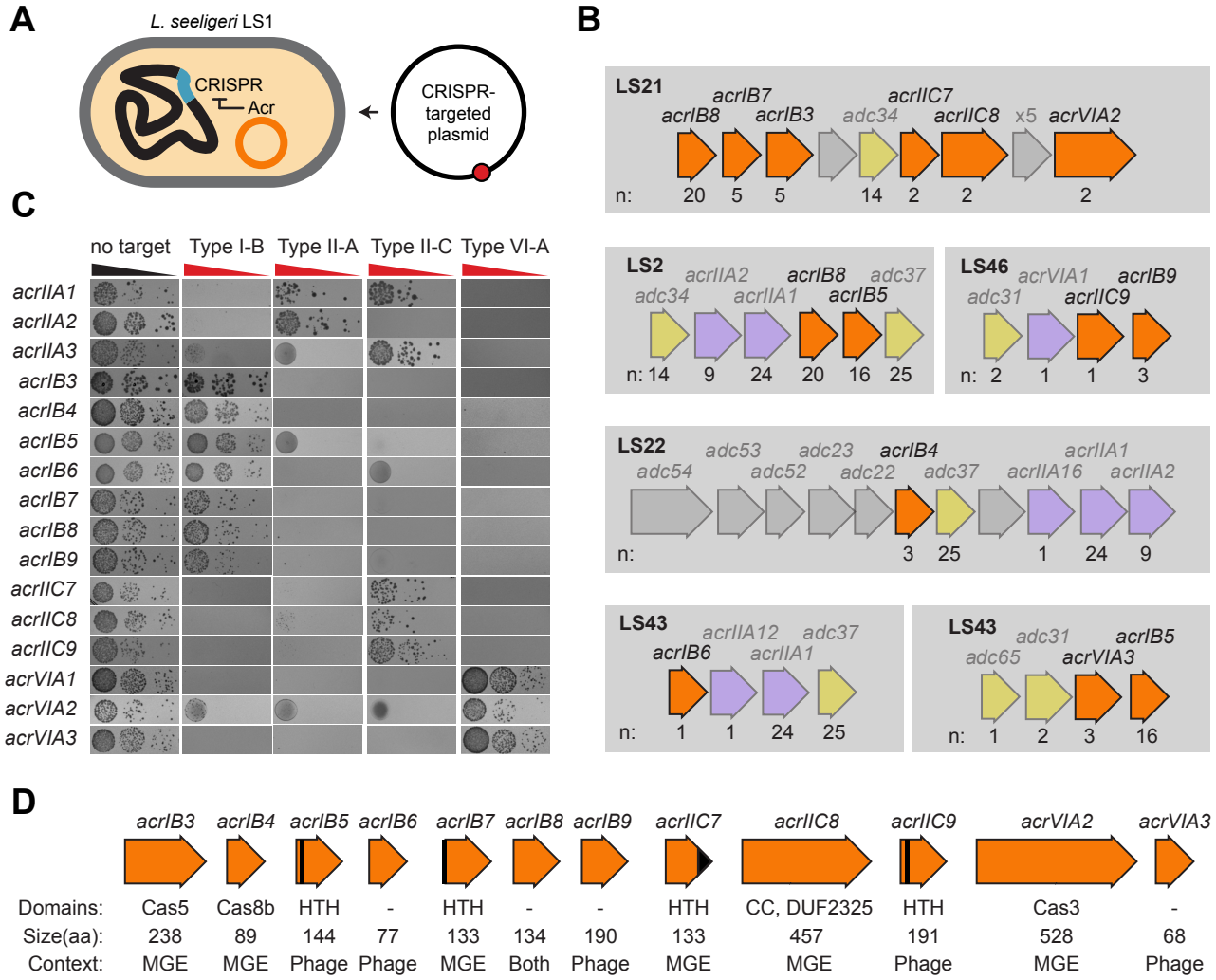

Figure 2. Identification of 12 type I-B, II-C, and VI-A anti-CRISPR families (A) Schematic of strategy to test Acr candidates. Acrs were expressed from a plasmid and introduced into strain LS1 harboring an active CRISPR-Cas system, then challenged with a target plasmid. **(B)** Genetic loci encoding known and novel Acrs. Known Acrs shown in purple. Anti-defense candidate genes used in prediction of Acr loci shown in yellow. Novel Acrs with activity demonstrated here shown in orange. n, number of instances of indicated gene in *L. seeligeri* collection. **(C)** Inhibition spectrum of tested Acrs. Each Acr candidate was tested against all four CRISPR-Cas systems in a plasmid targeting assay. **(D)** Acrs discovered in this study. Predicted protein domains noted, with HTH (helix-turn-helix) domains depicted in black. MGE, mobile genetic element.

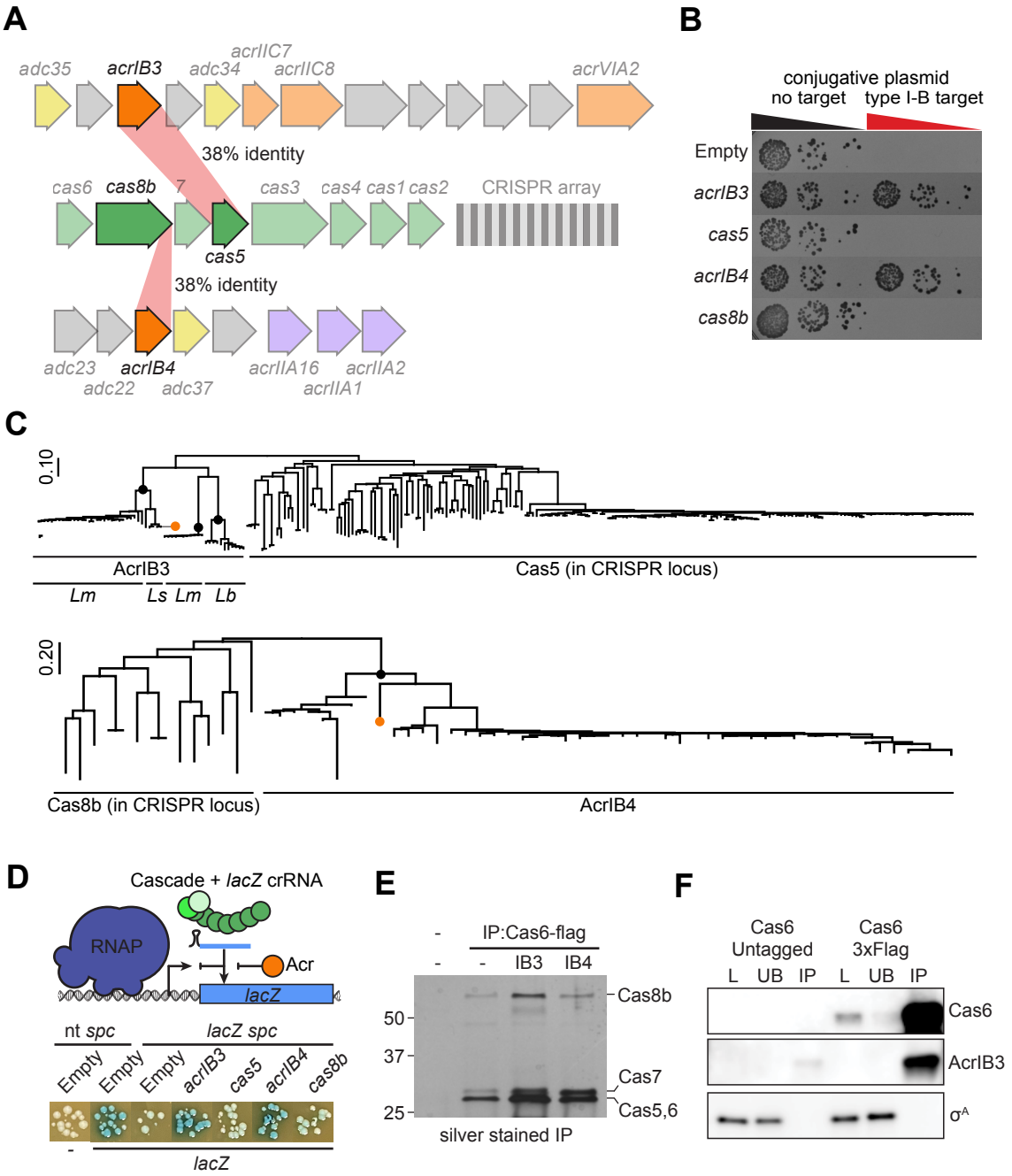

Figure 3. AcrIB3 and AcrIB4 are Cas protein homologs that inhibit type I-B CRISPR immunity (A) Schematic of genetic loci encoding AcrIB3 and AcrIB4 (opaque orange) and type I-B CRISPR-Cas locus. Percent sequence identity between AcrIB3 and Cas5, and AcrIB4 and the CTD of Cas8b are noted. **(B)** Plasmid targeting assay demonstrating that expression of AcrIB3 and AcrIB4, but not their cognate Cas proteins Cas5 and Cas8b, inhibits type I-B CRISPR immunity. **(C)** Predicted phylogeny of AcrIB3 and AcrIB4 homologs uncovered by BLAST search. Black circles indicate nodes with >80% boostrap support. Orange circles indicate Acrs characterized experimentally. Scale bar indicates branch length (AU). **(D)** CRISPRi *lacZ* silencing assay using a nuclease-deficient CRISPR system, demonstrating that both AcrIB3 and AcrIB4 inhibit target DNA recognition by Cascade. **(E)** Silver stain analysis of Cas6-3xFlag (or untagged) immunoprecipitate fractions in the presence or absence of Acrs. Molecular weight marker, kDa. **(F)** Co-immunoprecipitation of His6-AcrIB3 and Cas6-3xFlag. The housekeeping sigma factor σ^A is shown as a non-interacting control. L, load, UB, unbound, IP, immunoprecipitate.

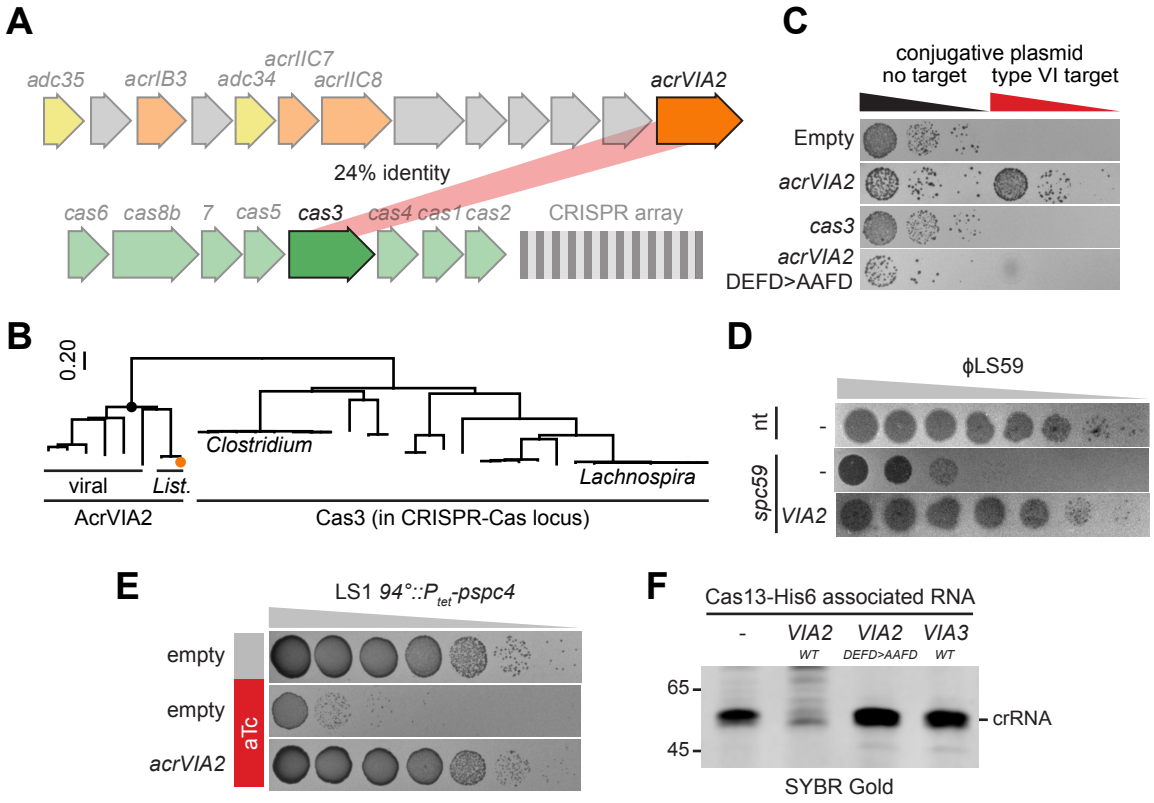

Figure 4. AcrVIA2 is a Cas3 homolog that inhibits type VI-A CRISPR immunity (A) Schematic of genetic loci encoding AcrVIA2 (opaque orange) and type I-B CRISPR-Cas locus. Percent sequence identity between AcrVIA2 and Cas3 is noted. **(B)** Predicted phylogeny of AcrVIA2 homologs uncovered by BLAST search. Black circle indicates node with 100% bootstrap support. Orange circle indicates experimentally characterized Acr. Scale bar indicates branch length (AU). (**C**) Plasmid targeting assay demonstrating that expression of AcrVIA2, but not Cas3 or an AcrVIA2 DEAD-box mutant allele, inhibits type VI-A CRISPR immunity. **(D)** Plaque assay demonstrating that AcrVIA2 inhibits type VI-A immunity against a phage target. nt, non-targeting, spc59, spacer targeting an early lytic transcript of ϕLS59. **(E)** AcrVIA2 inhibits *trans*-RNase activity of Cas13 in vivo. Strain LS1 harboring an aTc-inducible type VI-A protospacer, plus AcrVIA2, was plated on media with or without aTc, as indicated. **(F)** The effect of AcrVIA2 on crRNA associated with affinity-purified Cas13-his6. Nucleotide molecular weight marker shown.

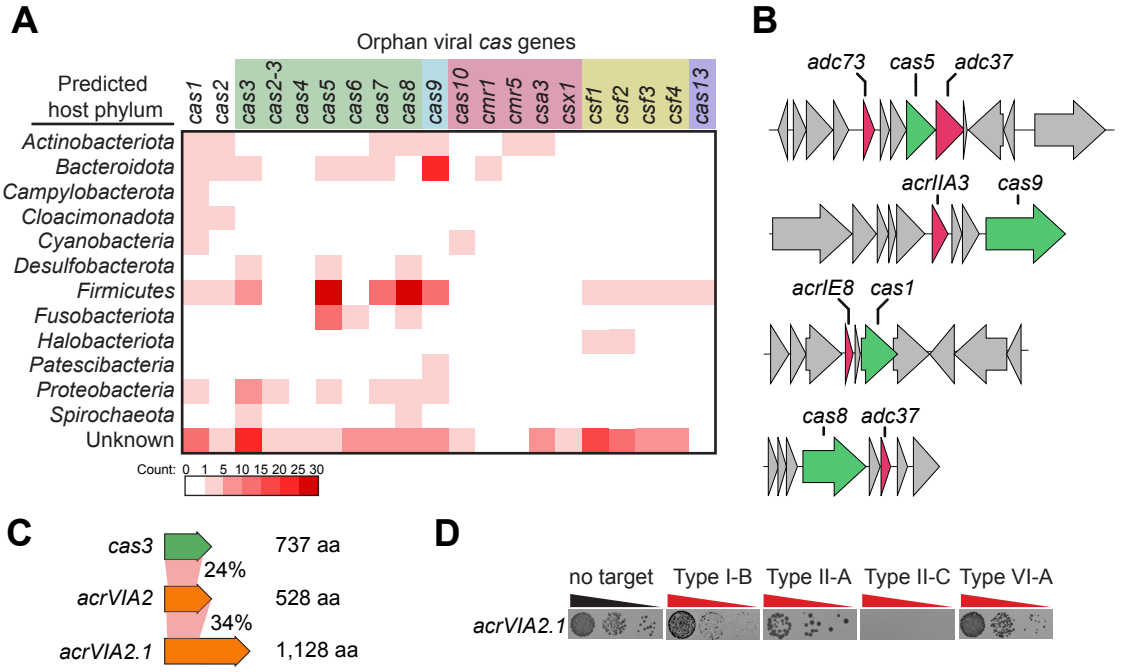

Figure 5. Diverse viral *cas* genes reside in putative anti-defense loci (A) Frequency of orphan viral *cas* genes found in the IMGVR database, organized by Cas protein query and predicted viral host phylum. Cas queries are colored by CRISPR type (green - type I; blue - type II; pink - type III; yellow - type IV; purple - type VI). **(B)** Example loci schematics for viral *cas* genes found in the vicinity of known anti-CRISPRs or other predicted anti-defense genes. **(C)** Schematic showing percent amino acid identity between *L. seeligeri* Cas3, the indicated Acrs, and each other, along with protein lengths. (**D**) Plasmid targeting assay demonstrating the CRISPR inhibition spectrum of viral Cas3 protein.

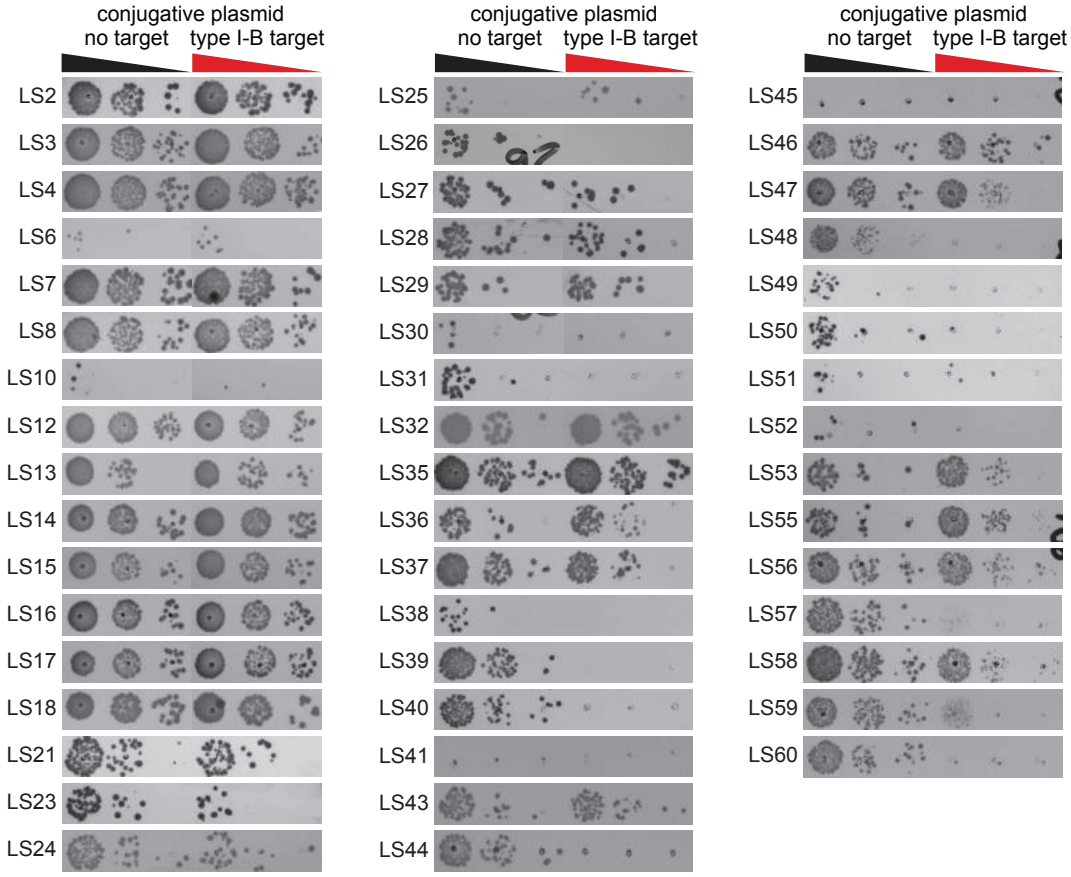

Figure S1. Variation in *L. seeligeri* strain background affects type I-B CRISPR-Cas immunity. Plasmid targeting assay in which the indicated L. seeligeri strains were first transformed with a chromosomally integrated type I-B CRISPR-Cas system equipped with a spacer targeting a conjugative plasmid, then challenged with either a non-target plasmid (left columns) or plasmid containing a target protospacer (right columns).

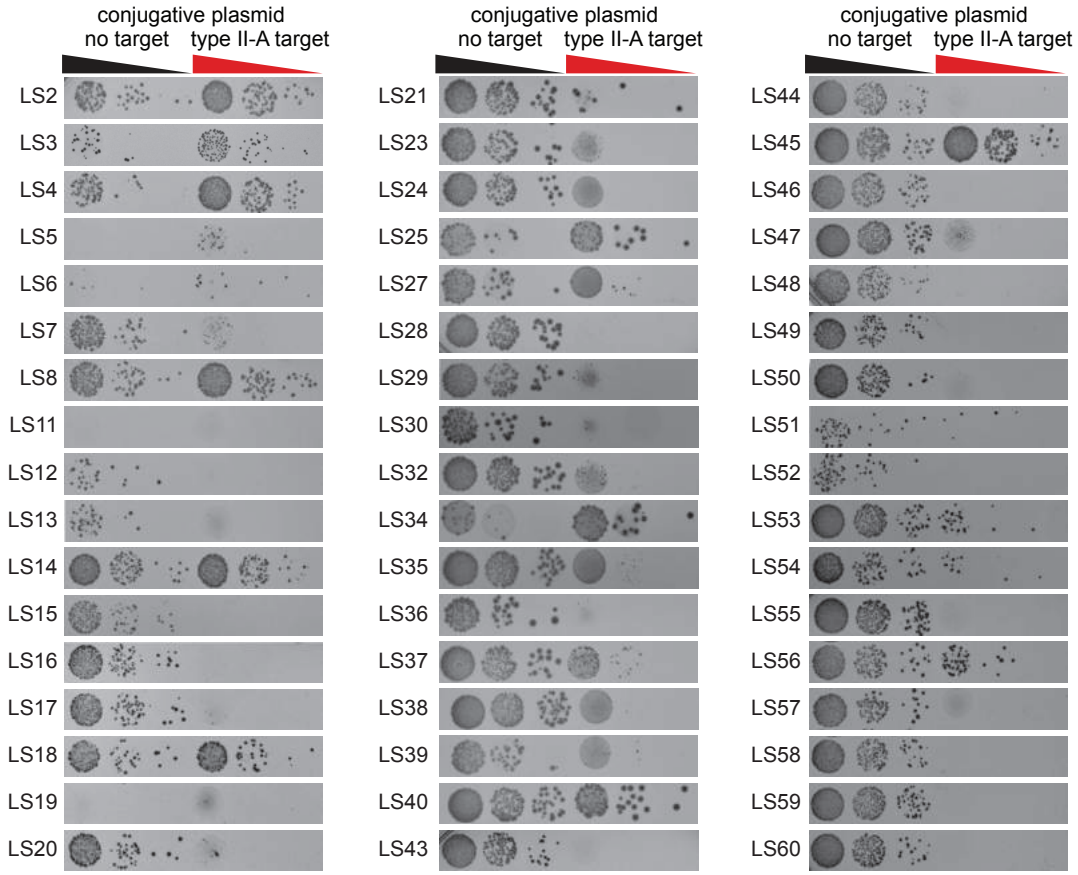

Figure S2. Variation in *L. seeligeri* strain background affects type II-A CRISPR-Cas immunity. Plasmid targeting assay in which the indicated L. seeligeri strains were first transformed with a chromosomally integrated type II-A CRISPR-Cas system equipped with a spacer targeting a conjugative plasmid, then challenged with either a non-target plasmid (left columns) or plasmid containing a target protospacer (right columns).

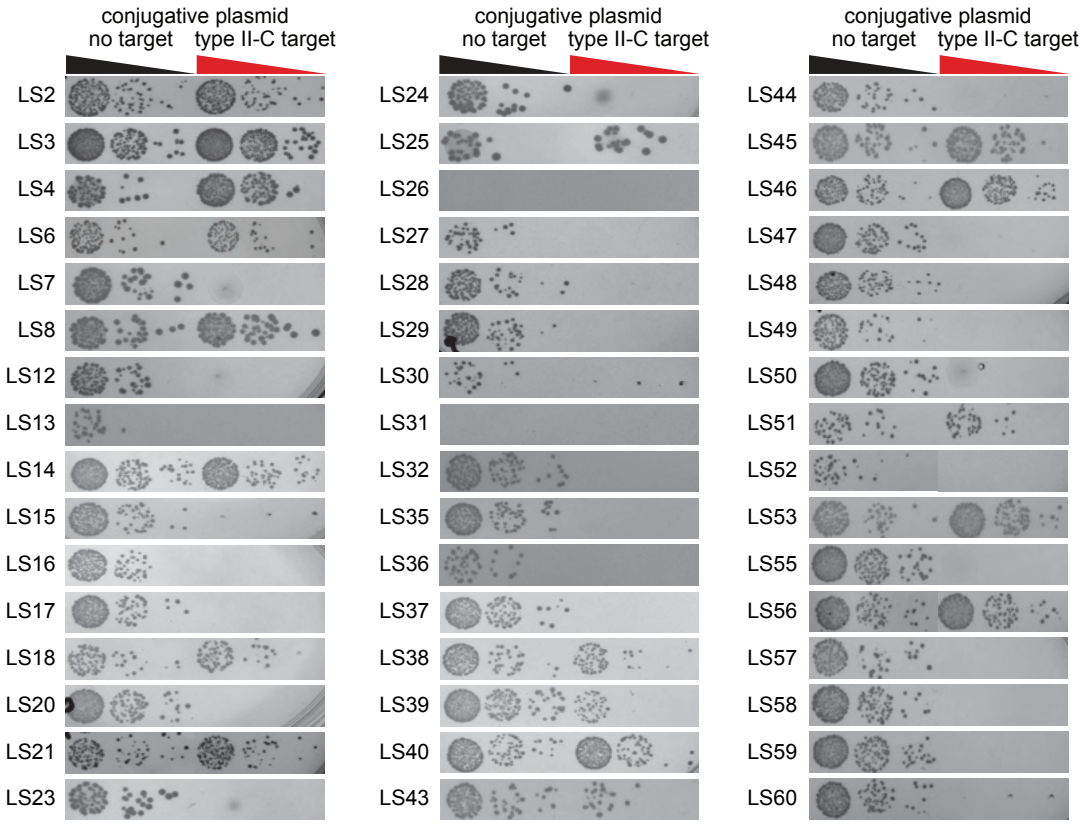

Figure S3. Variation in *L. seeligeri* strain background affects type II-C CRISPR-Cas immunity. Plasmid targeting assay in which the indicated L. seeligeri strains were first transformed with a chromosomally integrated type II-C CRISPR-Cas system equipped with a spacer targeting a conjugative plasmid, then challenged with either a non-target plasmid (left columns) or plasmid containing a target protospacer (right columns).

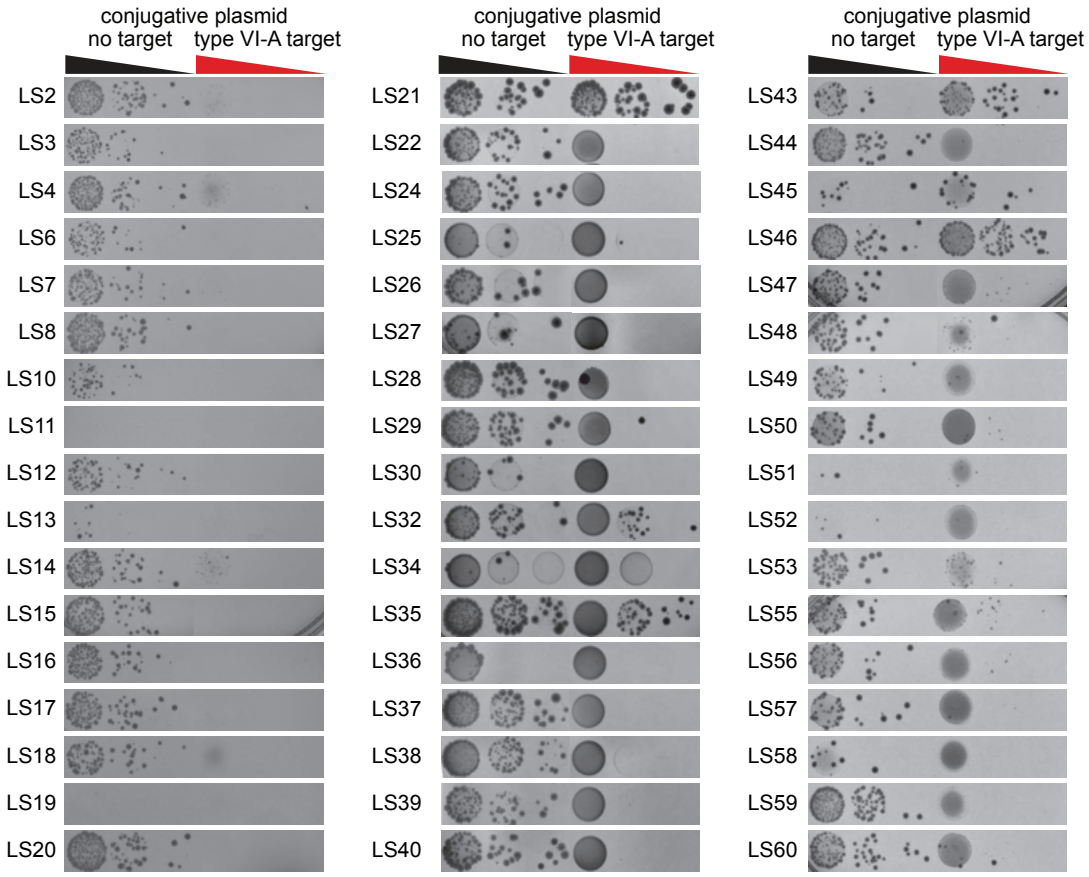

Figure S4. Variation in *L. seeligeri* strain background affects type VI-A CRISPR-Cas immunity. Plasmid targeting assay in which the indicated L. seeligeri strains were first transformed with a chromosomally integrated type VI-A CRISPR-Cas system equipped with a spacer targeting a conjugative plasmid, then challenged with either a non-target plasmid (left columns) or plasmid containing a target protospacer (right columns).

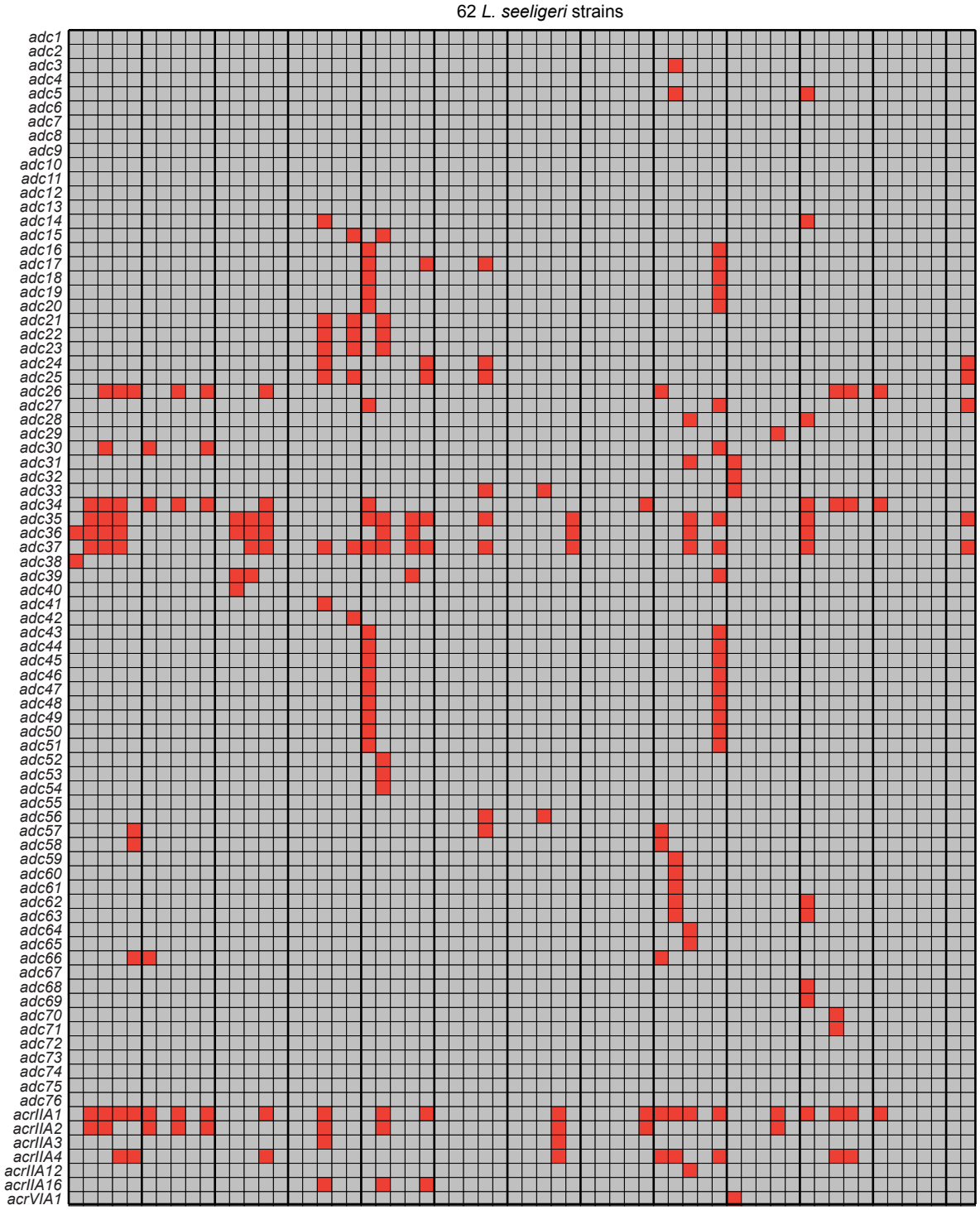

Figure S5. Anti-defense candidate (*adc*) gene occurrence across 62 strains of *L. seeligeri*. Each row correponds to either a known anti-CRISPR gene or a particular anti-defense candidate gene identified as frequently encoded nearby *acr* genes or nearby other well-established anti-defense canddiates. Each column corresponds to an individual *L. seeligeri* strain genome. Filled red boxes indicate occurence of a putative anti-defense gene in a particular strain.

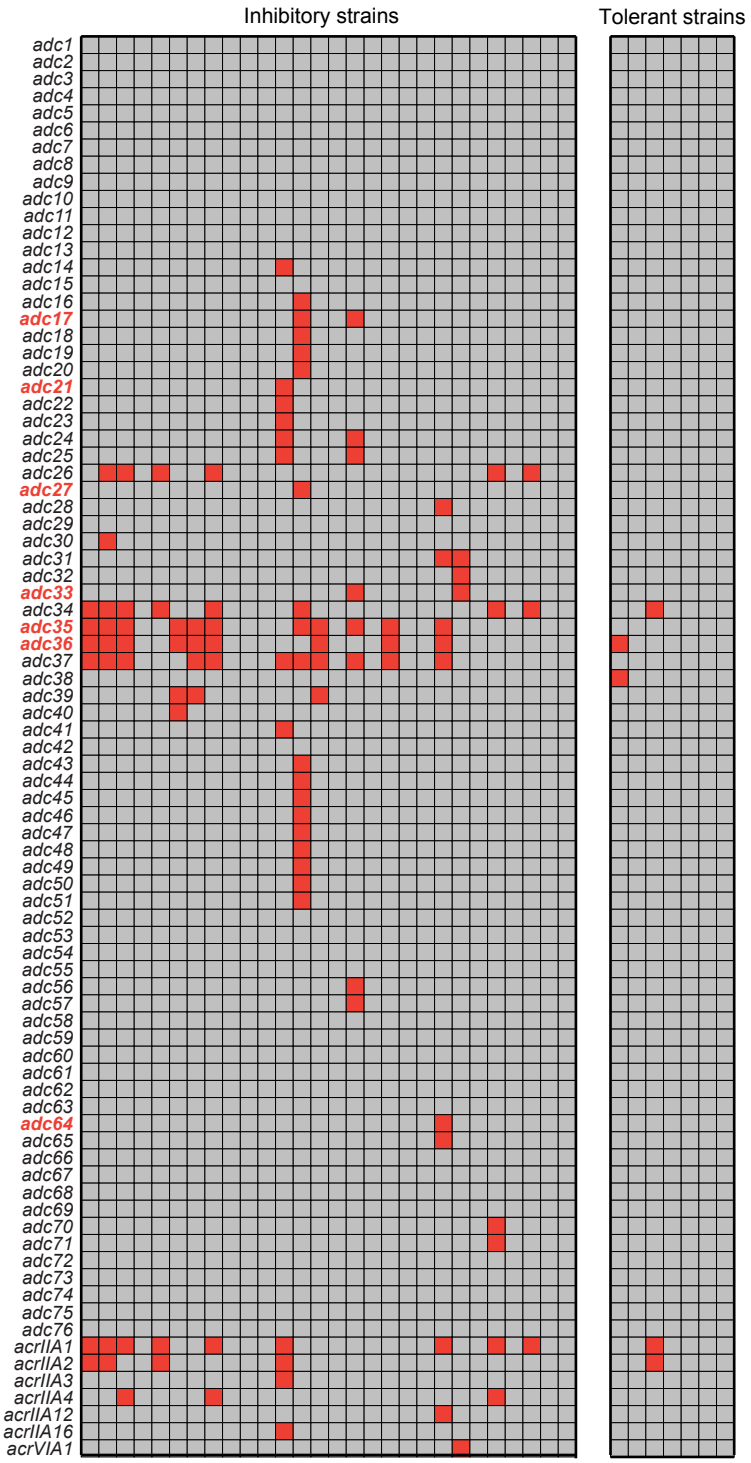

Figure S6. Anti-defense candidate (*adc*) gene occurrence among *L. seeligeri* strains that inhibit (or tolerate) type I-B CRISPR immunity. Each row correponds to either a known anti-CRISPR gene or a particular anti-defense candidate gene identified as frequently encoded nearby *acr* genes or nearby other well-established anti-defense canddiates. Each column corresponds to an individual *L. seeligeri* strain genome. The group of columns on the left indicate strains that inhibited type I-B CRISPR immunity in the plasmid targeting assay shown in Fig. 1, while the group on the right tolerated type I-B immunity. Filled red boxes indicate occurence of a putative anti-defense gene in a particular strain. Gene names in red indicate experimentally validated type I-B Acrs from this study.

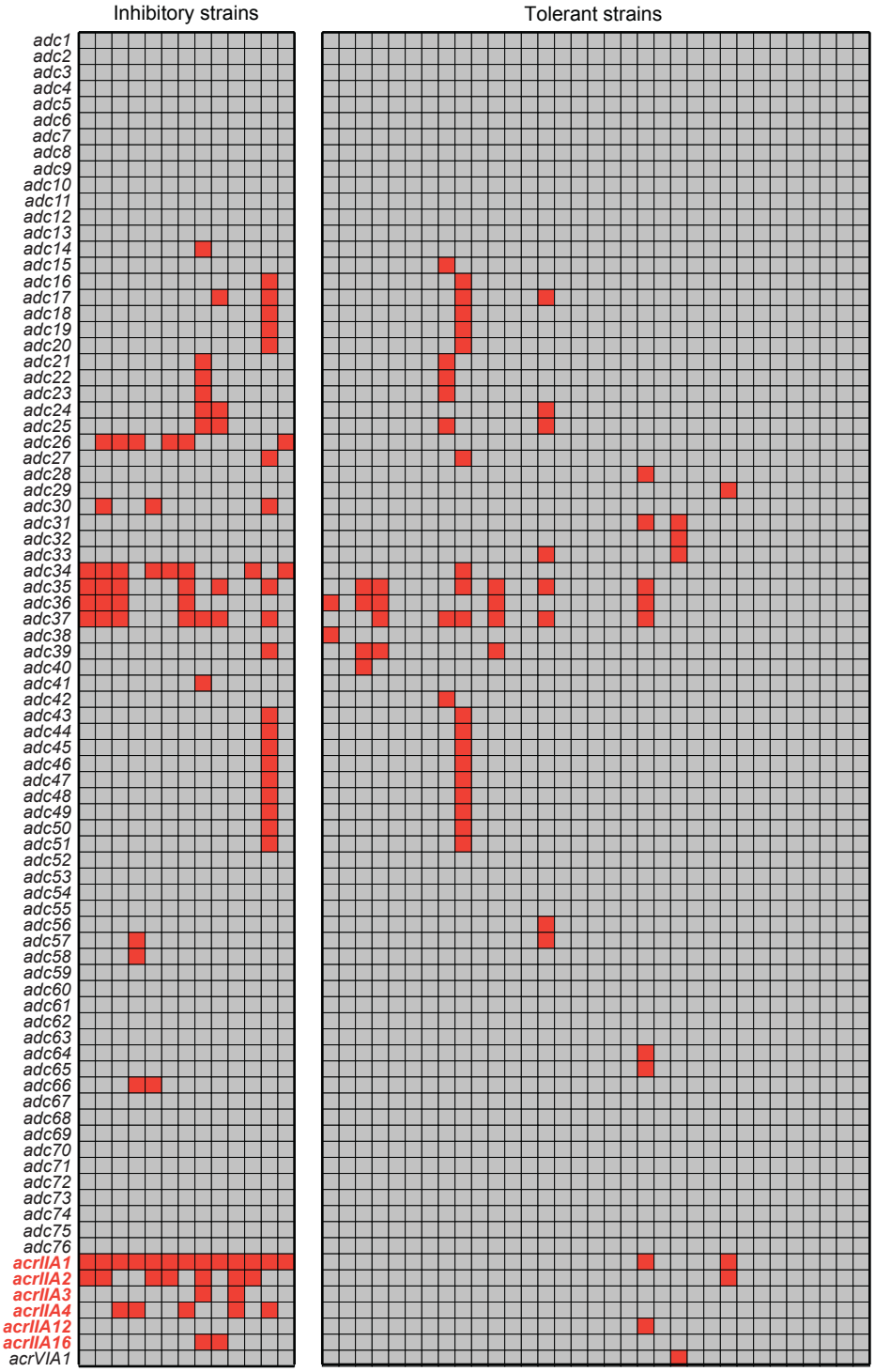

Figure S7. Anti-defense candidate (*adc*) gene occurrence among *L. seeligeri* strains that inhibit (or tolerate) type II-A CRISPR immunity. Each row correponds to either a known anti-CRISPR gene or a particular anti-defense candidate gene identified as frequently encoded nearby *acr* genes or nearby other well-established anti-defense canddiates. Each column corresponds to an individual *L. seeligeri* strain genome. The group of columns on the left indicate strains that inhibited type II-A CRISPR immunity in the plasmid targeting assay shown in Fig. 1, while the group on the right tolerated type II-A immunity. Filled red boxes indicate occurence of a putative anti-defense gene in a particular strain. Gene names in red indicate experimentally validated type II-A Acrs.

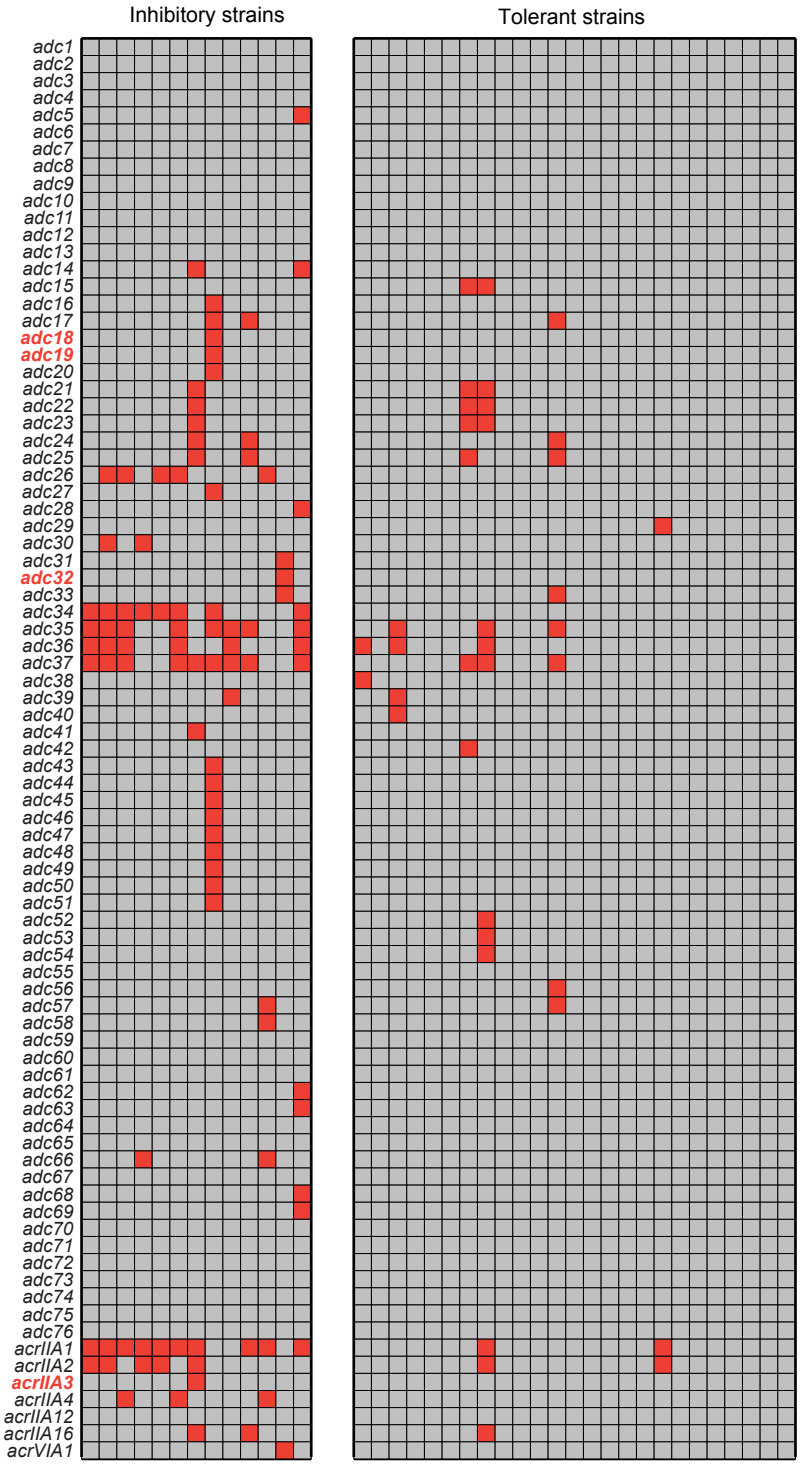

Figure S8. Anti-defense candidate (*adc*) gene occurrence among *L. seeligeri* strains that inhibit (or tolerate) type II-C CRISPR immunity. Each row correponds to either a known anti-CRISPR gene or a particular anti-defense candidate gene identified as frequently encoded nearby *acr* genes or nearby other well-established anti-defense canddiates. Each column corresponds to an individual *L. seeligeri* strain genome. The group of columns on the left indicate strains that inhibited type II-C CRISPR immunity in the plasmid targeting assay shown in Fig. 1, while the group on the right tolerated type II-C immunity. Filled red boxes indicate occurence of a putative anti-defense gene in a particular strain. Gene names in red indicate experimentally validated type II-C Acrs from this study.

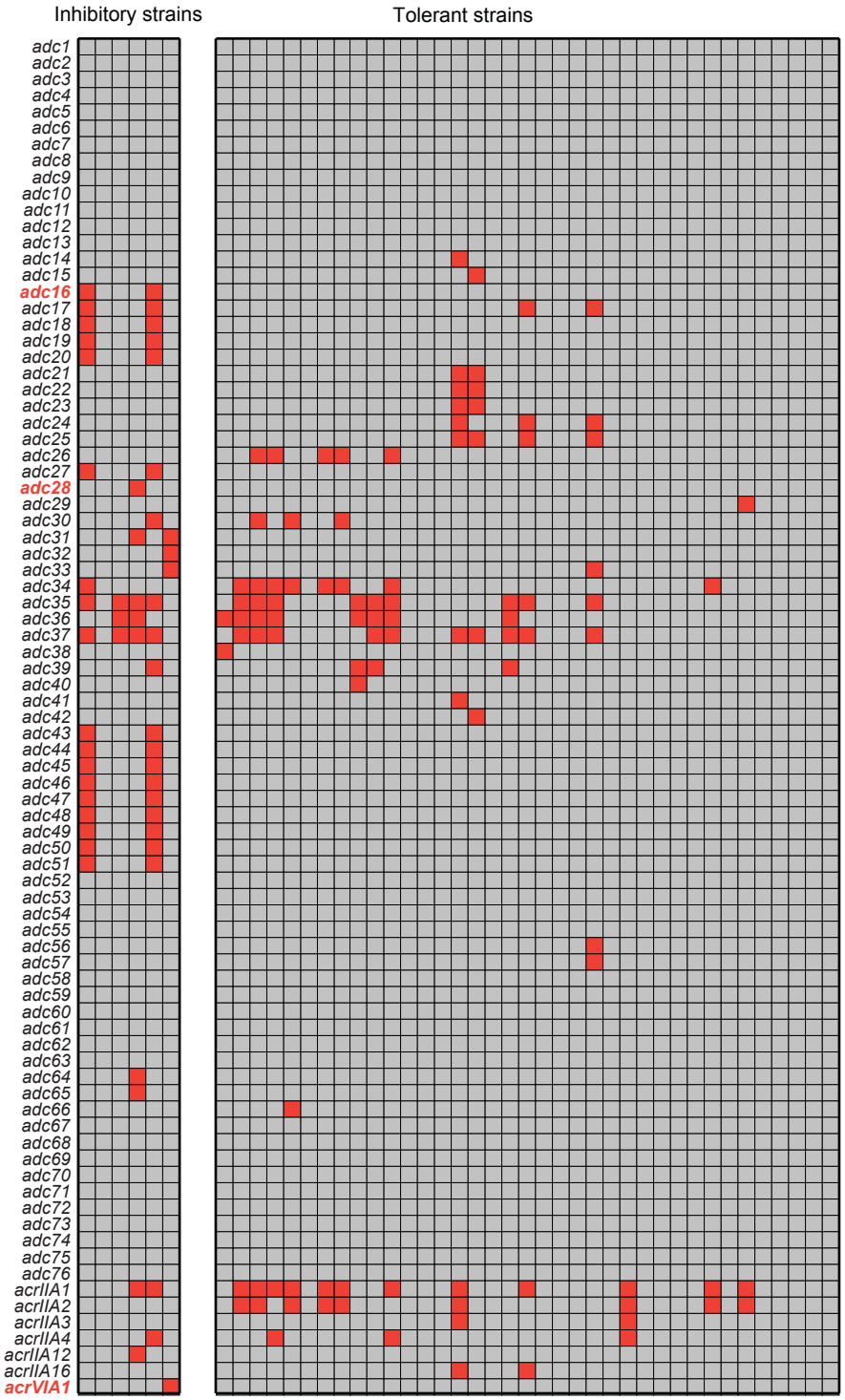

Figure S9. Anti-defense candidate (*adc*) gene occurrence among *L. seeligeri* strains that inhibit (or tolerate) type VI-A CRISPR immunity. Each row correponds to either a known anti-CRISPR gene or a particular anti-defense candidate gene identified as frequently encoded nearby *acr* genes or nearby other well-established anti-defense canddiates. Each column corresponds to an individual *L. seeligeri* strain genome. The group of columns on the left indicate strains that inhibited type VI-A CRISPR immunity in the plasmid targeting assay shown in Fig. 1, while the group on the right tolerated type VI-A immunity. Filled red boxes indicate occurence of a putative anti-defense gene in a particular strain. Gene names in red indicate experimentally validated type VI-A Acrs from this study.

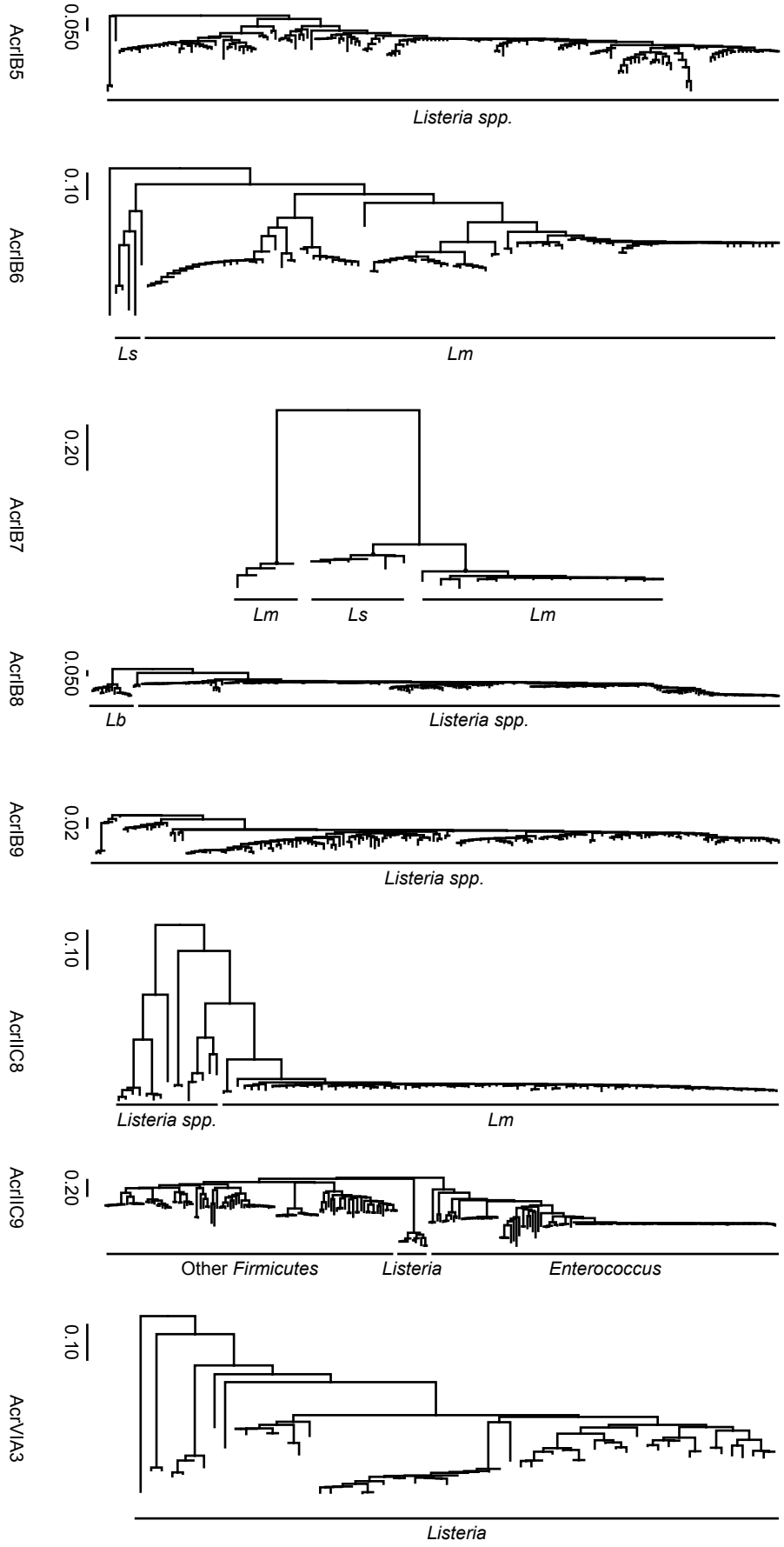

Figure S10. Predicted phylogeny of newly discovered type I-B, II-C, and VI-A anti-CRISPR proteins. Predicted phylogeny of Acr homologs uncovered by BLAST search. Scale bar indicates branch length (AU). See Fig. 3 for predicted phylogeny of AcrIB3 and AcrIB4 homologs. See Fig. 4 for predicted phylogeny of AcrVIA2 homologs.

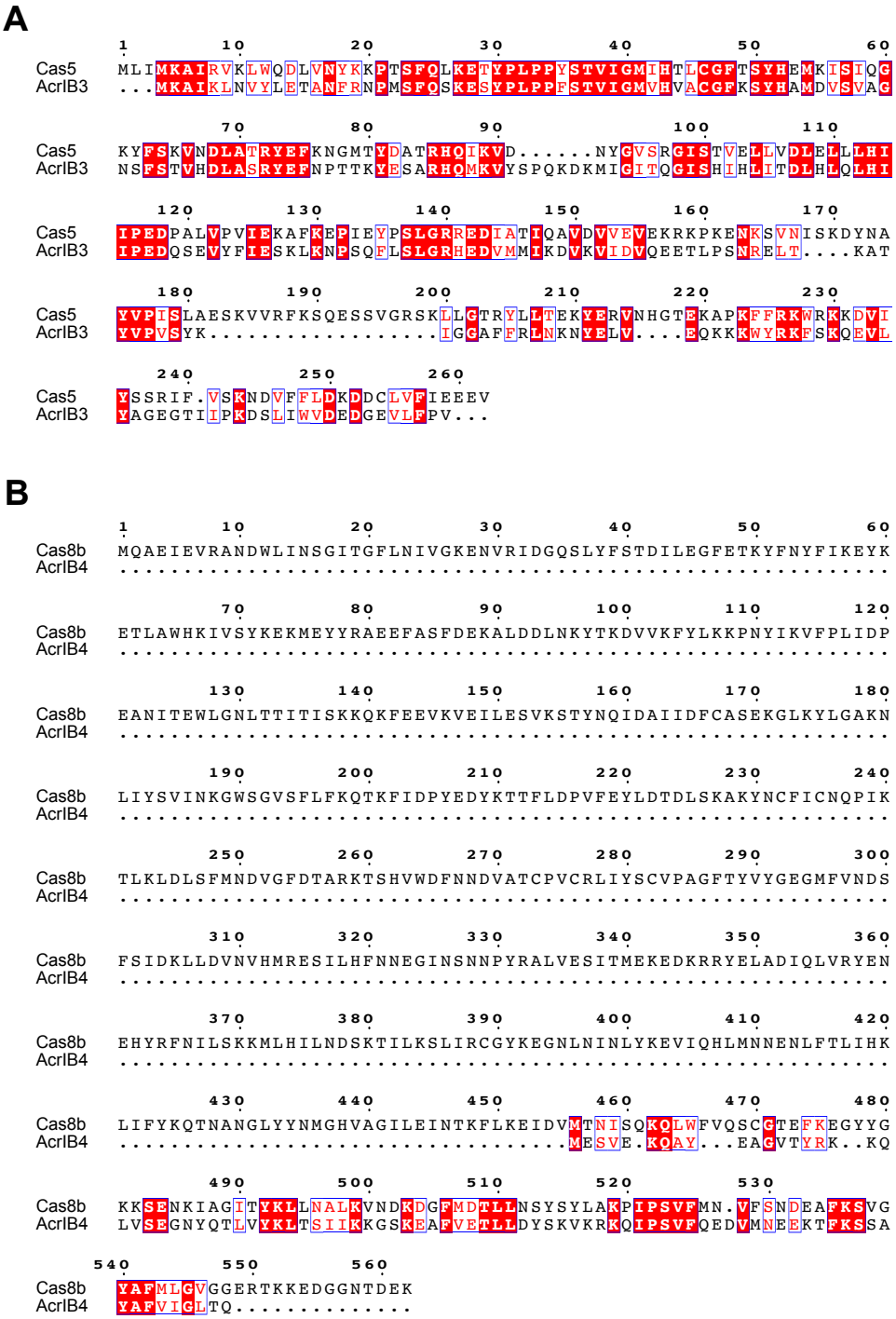

Figure S11. Sequence alignment of type I-B Acrs and type I-B Cas proteins (A) Sequence alignment of AcrIB3 and Cas5 from *L. seeligeri* strain LS1. Identical residues are highlighted in red, while similar residues are in red text with blue outlines. **(B)** As for (A), but for AcrIB4 and Cas8b.

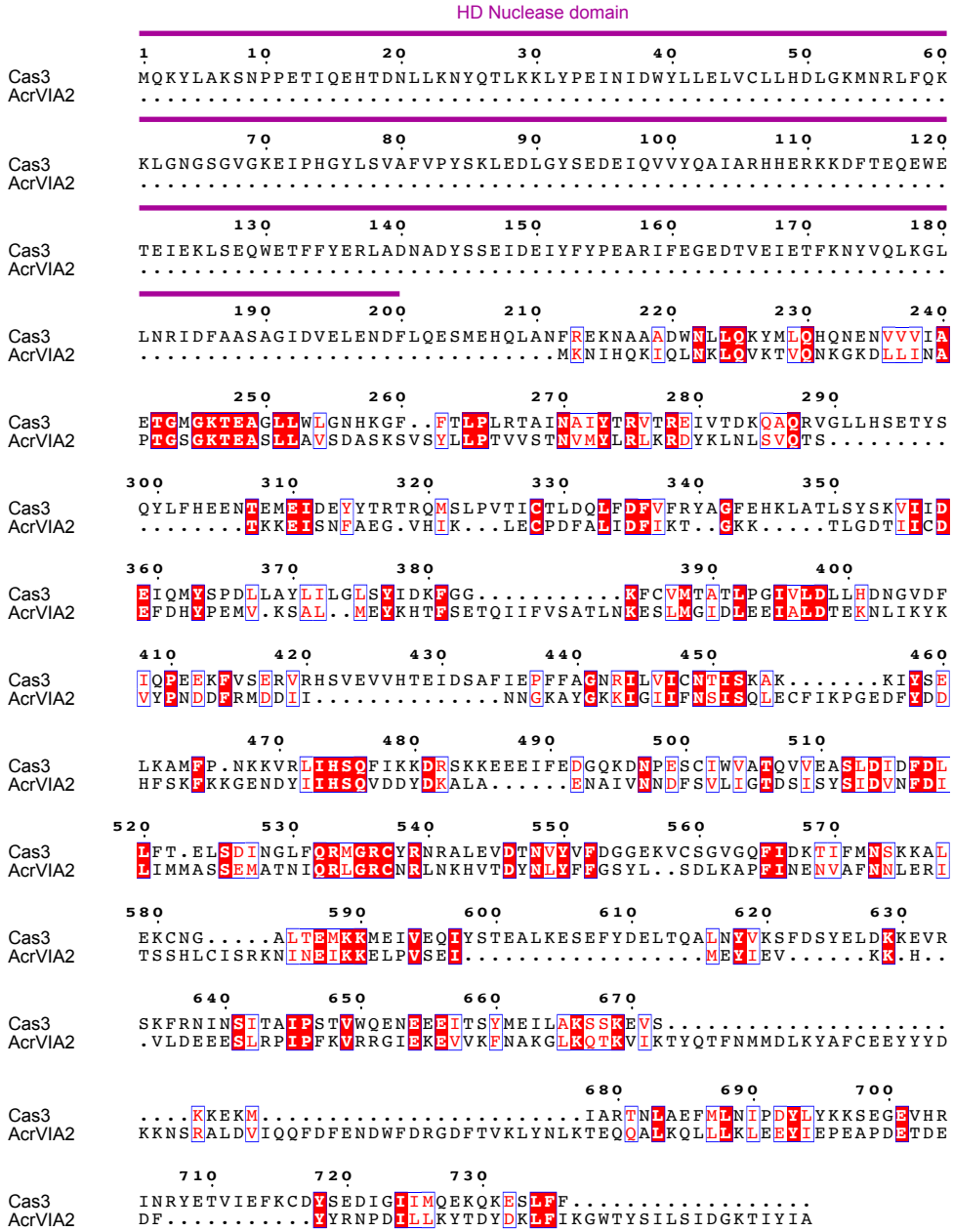

Figure S12. Sequence alignment of AcrVIA2 and the type I-B helicase-nuclease Cas3. Sequence alignment of AcrVIA2 and Cas3 from *L. seeligeri* strain LS1. Identical residues are highlighted in red, while similar residues are in red text with blue outlines.

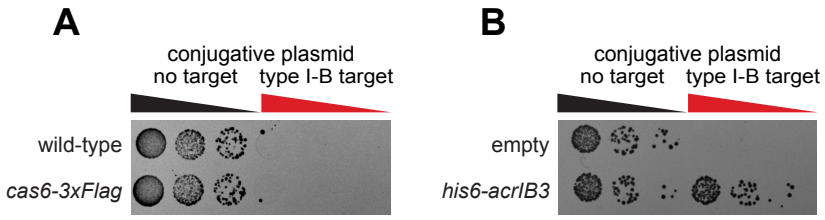

Figure S13. Functionality of affinity-tagged Cas proteins (A) Cas6-3xFlag functions in immunity against a plasmid containing a protospacer recognized by the type I-B CRISPR system. **(B)** His6-AcrIB3 functions in inhibition of type I-B CRISPR immunity in the plasmid targeting assay.

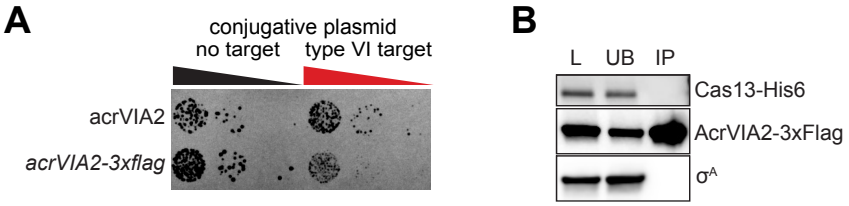

Figure S14. No detectable interaction between AcrVIA2 and Cas13 (A) AcrVIA2-3xFlag is partially functional in inhibition of immunity against a plasmid expressing an RNA protospacer recognized by the type VI-A CRISPR system. **(B)** No detectable co-immunoprecipitation of Cas13-his6 and AcrVIA2-3xFlag. The housekeeping sigma factor σ^A is shown as a non-interacting control. L, load, UB, unbound, IP, immunoprecipitate.

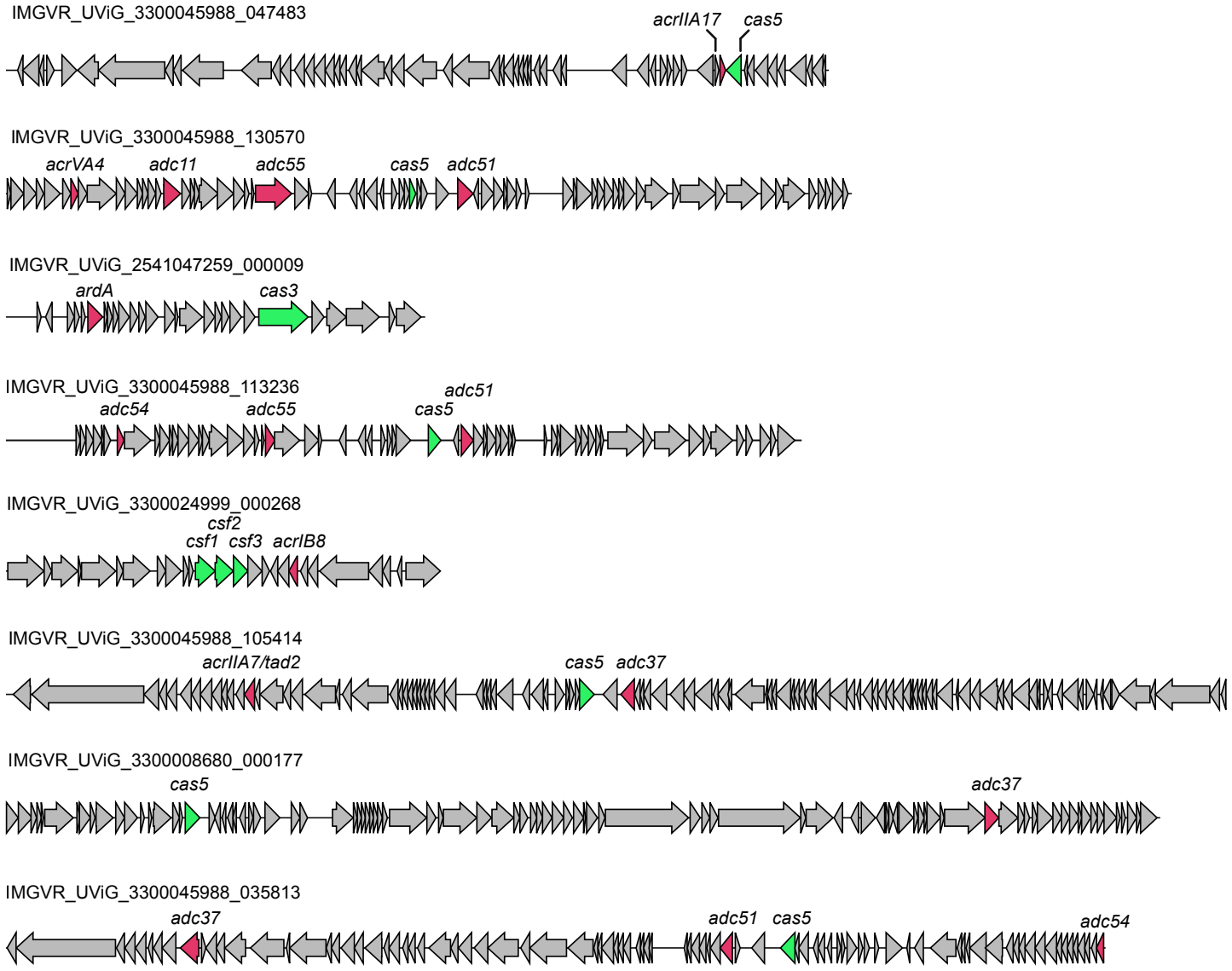

Figure S15. Orphan viral cas genes in the vicinity of known *acr* genes or putative anti-defense candidates (*adc*). Orphan viral cas gene homologs detected in the IMGVR database (green) that are located nearby known anti-CRISPR genes or putative anti-defense candidates (red). The unique viral genome identifer (UViG) number is shown for each locus. See other examples in Fig. 5B.